



Correlation between Hierarchical Structure of Crystal Networks and Macroscopic Performance of Mesoscopic Soft Materials and Engineering Principles

Journal:	<i>Chemical Society Reviews</i>
Manuscript ID:	CS-REV-01-2015-000074.R2
Article Type:	Review Article
Date Submitted by the Author:	04-Jul-2015
Complete List of Authors:	Lin, Naibo; Xiamen University, Liu, Xiang-Yang; National University of Singapore, Physics

REVIEW ARTICLE

Correlation between Hierarchical Structure of Crystal Networks and Macroscopic Performance of Mesoscopic Soft Materials and Engineering Principles

Cite this: DOI: 10.1039/x0xx00000x

Received 00th January 2012,
Accepted 00th January 2012

DOI: 10.1039/x0xx00000x

www.rsc.org/

Naibo Lin,^a Xiang Yang Liu^{b, a *}

This review is to explore how the concepts and ideas of crystallization can be further extended and applied to the field of mesoscopic soft materials. It concerns the structural characteristics vs the macroscopic performance, and the formation mechanism of crystal networks. Although this subject can be discussed in a broad sense across the area of mesoscopic soft materials, our main concentration are focused on supramolecular materials, spider and silkworm silks, biominerals, etc. Firstly, the occurrence of hierarchical structure, c.f. crystal network and domain network structures, will facilitate the formation kinetics of mesoscopic phase, and boost up the macroscopic performance of materials in some cases (i.e. spider silk fibres). Secondly, the structure and performance of materials can be correlated in some way by the four factors: *topology*, *correlation length*, *symmetry/ordering*, and *strength of association* of crystal networks. Moreover, four different kinetic paths of crystal network formation are identified, namely, *one-step process of assembly*, *two-step process of assembly*, *mixed mode of assembly* and *foreign molecule mediated assembly*. Based on the basic mechanisms of crystal nucleation and growth, the formation of crystal networks, i.e. *crystallographic mismatch* (or *noncrystallographic*) branching (tip branching, fibre side branching), fibre/polymeric side merging etc., are reviewed. This allows the rational design and construction of crystal networks in supramolecular materials. In this context, the (re-) construction of hierarchical crystal network structure can be implemented by thermal, participate, chemical, sonication stimuli etc. As another important class of soft materials, the unusual mechanical performance of spider and silkworm silk fibres are reviewed in comparison with the regenerated silk protein derivatives. It follows that the much larger breaking stress and unusual breaking strain of spider silk fibres vs silkworm silk fibres are interpreted according to the synergistically correlated hierarchical structures of domain and crystal networks, which can be quantified by the hierarchical structural correlation and the four structural parameters. Based on the concept of crystal networks, the new understandings acquired will transfer the research and engineering of mesoscopic materials, in particular, soft functional materials, to a new phase.

1. Introduction

The structure and performance of materials are the two sides of a coin. They are considered as the basic two elements of “Yin” and “Yang” in the Taoism. On one hand, the structure of materials determines the performance. On the other hand, the outstanding performance of materials is attributed to some specific structures (Fig.1). Crystals as typical bulk functional materials have been attracting people’s interests for centuries.¹ Conventionally, the structural units in crystalline materials are atoms, natural and synthetic molecules.² Recent researches reveal that for many new functional materials, *the macroscopic behaviour begins to manifest itself not at the atomic or nanoscale but at the mesoscale*.³ *With our recently acquired knowledge of the rules of nature that govern the atomic and nano scales, we are well positioned to unravel and control the complexity that determines functionality at the mesoscale*.³ Therefore, the ability to predict and control mesoscale phenomena and architectures is essential if atomic and molecular

knowledge is to blossom into a next generation of technology opportunities, societal benefits, and scientific advances.

Recently, crystal networks are found to be basic structural components of many soft materials,⁴ which have created significant interests across materials science. It follows that the relevancy of crystallization has been beyond the control of the size and the quality of bulk crystals or thin films, which has been the main concerns in the field of crystallization across the 20 century.⁵ It was discovered that the structure of associated crystallites-, or so-called crystal networks, plays a vital role in governing the properties or macroscopic behaviour of many materials, i.e. small molecule gels, polymeric gels, liquid crystals, and natural fibers (i.e. silk fibers), etc.⁶ It follows that in these cases, the basic building units are nanocrystalline (i.e. polymer gels and silk fiber) or partial crystalline. Due to the special structures and properties, these materials have been found in many fields including foods,⁷ cosmetics, drug delivery,⁸ tissue engineering,⁹ organic electronics,¹⁰ chemical sensing,¹¹ templates synthesis of materials¹² and art conservation,¹³ etc. We should notice that the outstanding performance of spider silk

fibers was found to be correlated with the hierarchical structure of crystal networks.¹⁴ Therefore, the comprehensive understanding on crystal networks, in particular, the structure/performance correlation is upmost importance. In this regard, if the perfection and the properties of bulk/thin single crystals are the main concern in traditional crystallization, how crystallites are associated with each other becomes the main concern for soft and hybrid materials. The key parameters that describe the way that crystallites are associated with each other in mesoscale determine the properties and macroscopic performance of materials while individual crystals and their properties become less important.¹³

The purpose of this review is to establish a comprehensive understanding on the role of crystal networks in soft materials performance, which are not considered in the classical-crystallization research. Our focus, therefore, will be devoted onto the basic features of crystal networks at the mesoscopic scale. This includes the classification and the formation of crystal networks which are evolved from traditional crystallization. In particular, how the crystallization theories and technologies can be extended beyond the classical domain, to describe the crystal network formation will be the main concern.

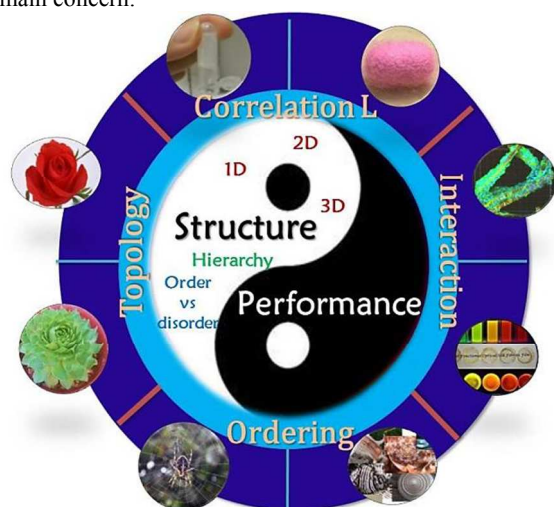


Fig. 1 The “Yin”~“Yang” fish of materials research: the structure and performance of materials can be considered as the basic two elements of “Yin” and “Yang” in the Taoism: On one hand, the structure of materials determines the performance. On the other hand, the outstanding performance of materials is the reflection of some specific structures. More specifically, such a connection can be described in some way by the four factors: *topology*, *correlation length (Correlation L)*, *interaction* and *ordering*.

We notice that as the overall strategy of materials science and engineering, “functionalization” is always the centre of concerns. In other words, to design and fabricate soft materials with desired functions and performance by (re-) constructing or tuning the mesoscopic materials should become the core of interests. This can be understood within the framework of the “yin”~“yang” fish of materials research (Fig. 1)⁴ In somewhat detail, the engineering of soft materials with some particular properties/performance can be achieved by fabricating the structure of the materials. This can be implemented by controlling the formation kinetics. This concerns the establishment of the correlation between the structure and performance of materials and the acquirement of formation kinetics of the materials. The later should allow us to control the structure in order to acquire the materials with some particular functionality. In this review, the acquired knowledge on the structure vs performance

relationship and the formation kinetics of the structure will be combined to implement the mesoscale engineering.

In this review, our concentration will then be focused on the correlation between crystal network structures and the performance of soft and hybrid materials etc. We will demonstrate how these traditional “non-crystalline” materials can be fabricated and how their properties can be optimized on the basis of crystal network engineering. Finally, we will show how the exceptional mechanical properties of animal silks, i.e. spider silk can be predicted based upon the knowledge of crystal networks. In this sense, the knowledge concerning crystal networks can also be extended to design and guide the fabrication of ultra-performance functional materials.

2. Mesoscopic Materials and Crystal Network

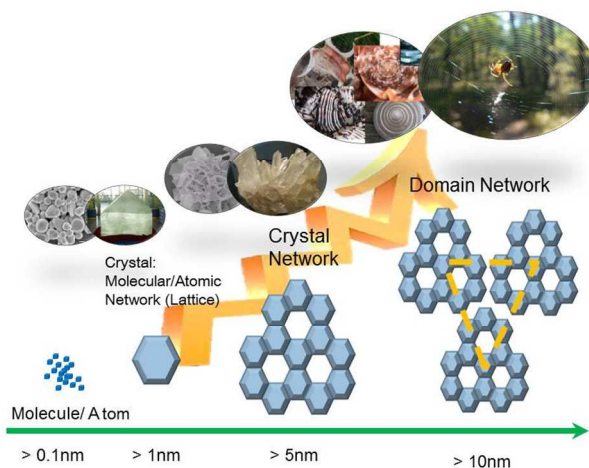


Fig. 2 Multilevel structure of crystal networks.

The properties of materials are determined to a large extent by the way how the building units are linked (i.e. structure and binding). The scale of such building units can be described as being between the size of a quantity of atoms (such as a molecule) and of materials measuring micrometers. The lower limit can also be defined as being the size of individual atoms. Objects have in common that they both contain a large number of atoms. Whereas average properties derived from its constituent materials describe macroscopic objects, as they usually obey the laws of classical mechanics, a mesoscopic object, by contrast, is affected by fluctuations around the average (Fig. 2).¹⁵

Recently, the challenging issues have further evolved as to how these nano building blocks can be assembled with each other. On the other hand, many materials, such as molecular gels, biominerals, animal silks, etc., are found to have nano building blocks as the basic building units, which are associated with each other in some ways to display some particular properties and performance of materials. As the way how the building blocks are associated with each other affects the performance of mesoscopic materials, the knowledge on the mesoscopic structure becomes particularly important.

In the case that the nano building units are crystallites, the association of the crystallites gives rise to crystal networks. The so-called crystal network can be defined as a group of crystallites associated with each other in some ways. The crystals in a crystal network can be associated with each other by themselves or crystals of different types, or non-crystalline molecules or an amorphous phase in one-dimensional, two-dimensional or three-dimensional

manners. Topologically, a crystal network can be described as a set of “nodes” interconnected by some “links”. The points refer to the joints where the connection occurs, while the lines correspond to the association or linkage between the points. Notice the links can be physical or non-physical connections.¹⁶ The performance of materials of this type is not only determined by the individual crystallites, but also by the way of crystallite association (crystal networks).

2.1. Hierarchical structure of crystal networks and description

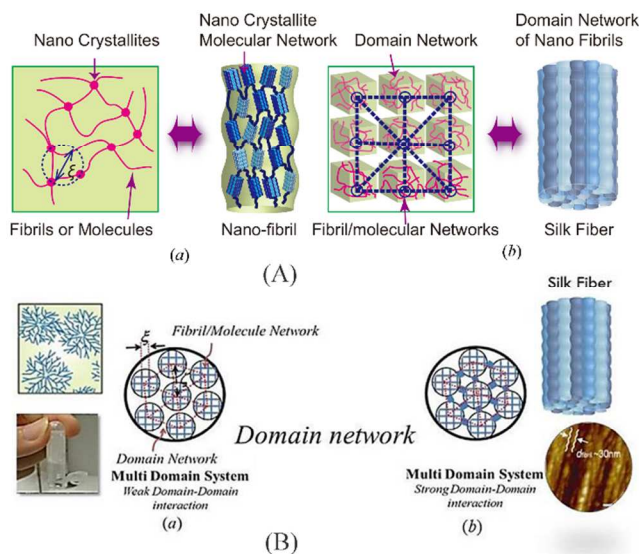


Fig. 3 (A) Comparison between the hierarchical network of soft materials and the silk fibre (a) “single” crystal network and nano-fibril in silk; (b) multi-domain fibre network and fibril bundle. (B) Schematic illustration of three typical hierarchical structures: (a) a multi domain system, the domain-domain interaction is weak or zero; (b) a multi domain system, the domain-domain interaction is strong or infinite. Modified from ref.¹⁷.

As illustrated by Fig.1, the structural factors that affect the performance of materials include the dimension, hierarchy, ordering etc. This holds for the materials with crystal network structures as well. According to the research in the past two decades, most crystal networks are of the hierarchical and fractal structure based on the Avrami equation.¹⁸ It has been identified that most crystal networks are of the statistical fractal characteristics. The *in-situ* measurement of the fractal growth and fractal or Hausdorff–Besicovitch dimension D_f crystal networks can be implemented by optical light scattering or rheological measurements. Compared with other methods, the rheological measurement can reveal the influence of both the small aggregates formed at the early stage and the larger aggregates at the late stage on the elasticity of the materials. One can refer to Ref.¹⁸ for more details. In the case of *N*-lauroyl-L-glutamic acid di-*n*-butylamide (GP-1) fiber network formation in solvents such as isostearyl alcohol,¹⁹ a gel formed at room temperature when cooling from 125 °C acquires the fractal dimension $D_f=2.4$. The change in fractal dimension can be applied to examine the change of crystal network structure: Lam et al. characterized the fractal dimension of 12-hydroxystearic acid (HSA) fibers formed in mineral oil as a function of cooling rate.²⁰ At slow cooling rates (i.e. less than 5 to 7 °C min⁻¹, long fibers were produced with a fractal dimension between 0.95 and 1.05 and for rapid cooling rates (i.e. greater than 5 to 7 °C min⁻¹) short branched fibers were produced with a fractal dimension between 1.15 and 1.32. This implies that at higher cooling

rates, the fibers are less linear and coincide with a higher degree of branching. The macroscopic properties of mesoscopic materials are largely determined by the hierarchical structure of crystal networks. The typical cases of crystal networks are summarized in Fig. 3.

In general, crystal networks can either occur in an entity (i.e. biominerals), or as a multi-phase (i.e. the solid/liquid) entity. In the latter case, the crystallite networks can effectively entrap and immobilize liquid in the meshes. This will give rise to soft materials which will behave like self-supporting soft solids.²¹

In most cases, a material does not constitute only a single crystal network, but a collection of disjoint individual networks, or more complex entities. A two level collection is referred to a multi-domain network (or domain network). At this level, the “nodes” of a multi-domain network are the individual crystal networks. Obviously, the “nodes” of a multi-domain network are the individual crystal networks. The “links” between the individual crystal networks can be physical contacts or weak interactions between neighbouring crystal networks (Fig.3A-b). Normally, a unit volume of a material constitutes a number of fibrous/crystalline networks, each of which can be considered as a single network. A group of single networks will form a higher level of networks, namely, “domain networks” (Fig. 3A).¹³ The macroscopic performance of mesoscopic materials is normally determined jointly by both the domain and the crystalline networks as well as the synergy between the different levels of networks. Fig. 3B illustrates two typical hierarchical structures: a multi domain network (a) with weak or zero domain-domain interactions; (b) with strong or infinite domain-domain interactions. In the following discussion, one can see that the systems with multiple spherulites belong to the case of Fig. 3 B(a) while spider silk and silkworm silk fibers belong to the case of Fig. 3B(b). Notice that if numerous crystal networks mutually interpenetrate and interlock with each other, they can be regarded as a “single” crystal network.

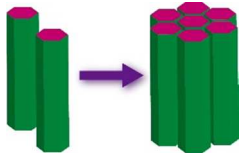


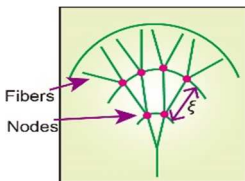
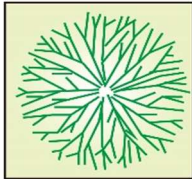

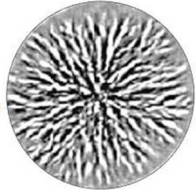
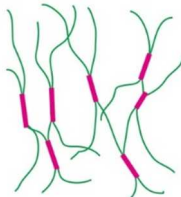
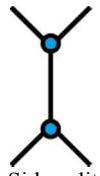

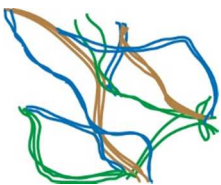
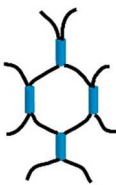
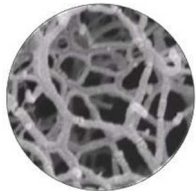
Regarding the materials of multi levels, the “links” between the adjacent fibrous networks are of particular importance for the mechanical performance of the soft materials having the hierarchical structures.²² The mechanical strength/stability of a multi-domain network material is determined by the “links” between the domains or the nodes in the fibrous networks and the synergy between the different levels of networks.²³ Apart from these, some other factors also play crucial roles.

The factors of both crystal and/or domain networks that determine the performance of mesoscopic materials can be summarized as follows:

- (1) *Topology*: the topology of nodes describes how the joints/points are associated with each other. In other words, it determines whether networks occur and how the compactness of the networks will be. Creating networks often start with topological modification.²⁴
- (2) *Correlation length*: the average of the distance between two physically or thermodynamically correlated points. For the fiber crystalline networks, this refers to the average of the distance between two adjacent points of networks.¹³
- (3) *Ordering/symmetry of building blocks*. In many cases, the crystallites of crystal networks are anisotropic. The symmetrical correlation or ordering of these crystallites determine the performance of the materials.¹⁷ For instance, the toughness of silk fibers and biominerals depends strongly on the ordering of crystallites.
- (4) *Strength of linkage or interactions*. Obviously, the stability of networks is directly correlated to the strength of linkage or interactions between the adjacent structural units. The linkage can be physical or chemical connections/bonding, virtual connections.^{13,17}

REVIEW ARTICLE

Table 1 Summary of some typical crystal networks²⁵

Typical network patterns	Simplified joints	Network Topologies	Examples
 <p>Side packing</p>	 <p>Side packing</p>	<p><i>Linear:</i> compact-fully connected Porous – partially connected.</p>	 <p>Biomaterials, hybrid materials etc.</p>
 <p>Fibers Nodes</p> 	 <p>Tip split</p>	<p><i>Star network 1:</i> Tree-like network</p>	 <p>Macromolecules, gels, biomaterials, organic and inorganic crystals etc.</p>
 <p>Side Merging/branching</p>	 <p>Side split</p>	<p><i>Star network 2:</i></p>	 <p>Macromolecules, gels, biomaterials, etc.</p>
 <p>Side Merging</p>	 <p>Closed Loop</p>	<p><i>Mesh network:</i> fully connected</p>	 <p>Macromolecules, gels, silks, etc.</p>

The images in Row 1 were reproduced with permission from Refs. ²⁶ and ²⁷. Copyright 2012 Springer, and copyright 2005 American Institute of Physics. The image in Row 3 was reproduced with permission from Ref. ²⁸. Copyright 2005 Springer. The left image in Row 4 was reprinted with permission from Ref. ²⁹. Copyright 2007 American Chemical Society. The right image in Row 4 was reprinted with permission from Ref. ³⁰. Copyright 2011, American Chemical Society.

REVIEW ARTICLE

2.2. Correlation between crystal networks and physical performance

2.2.1 Topology of crystal networks

Network topology refers to the arrangement of the various elements (links, nodes, etc.). Table 1 summarizes different topologies of crystal networks encountered frequently. Different topologies of networks often lead to the verification in compactness, rheological/mechanical properties and interfacial and macroscopic performance of mesoscopic materials. In other words, modifying the topology or pattern of crystal networks is one of the most effective ways to alter the properties and performance of mesoscopic materials.

In the following, some typical examples concerning the influence of crystal network pattern/topology on the macroscopic properties of materials are given.

(1) Rheological and gelation properties of soft solids

Soft materials of both fiber/crystal networks and a liquid phase have both the elastic properties of ideal solids and the viscous properties of Newtonian liquids (Fig. 4a). The complex modulus $G^* (= [(G')^2 + (G'')^2]^{1/2})$ is generally employed to characterize the rheological properties of a soft material. G' denotes the storage modulus (describing elasticity), and is mainly determined by the networks, and G'' the loss modulus (describing viscosity) and mainly determined by the fluid phase (Fig. 4a). G' is determined by the hierarchical structure of crystal networks.^{18a-c} Normally, a more fluid-like soft material has a higher G'' while a more solid-like soft material has a higher G' . A fluid-like soft material turning into a solid-like soft material is often considered as *gelation*. In a plot of G' , $G'' \sim$ time (t), the crossover point of G' and G'' is often regarded as the gelation point (t_g') (Fig. 4b). Alternatively, as the change of G' is attributed to the formation of mesoscopic networks which gives rise to the gelation of a fluid/liquid, another definition of the gelling point (t_g) can be taken as the point where G' reveals an abrupt increase (Fig. 4b).^{18a-c, 31}

The topology of crystal networks normally determines the rheological or gelation properties of the multiphase materials. Among the topologies of networks listed in Table 1, the star or mesh networks may gel a liquid phase easily while linear networks turn out to be more compact and of low gelling capability. For example, the dissolution of L-DHL (lanosta-8,24-dien-3 β -ol:24,25-dihydrolanosterol 56:44) in the organic solvent di-(2-ethyl-hexyl) phthalate (DIOP) at 110°C and cooling to room temperature will give rise to needle crystallites (side packing), and the formation of a paste-like slurry, (Fig. 4c). On the other hand, introducing some specific polymer additives (or *topological modifiers*, i.e. ethylene/vinyl acetate copolymer (EVACP)) may promote the formation of three dimensional interconnecting fiber networks (the change of the topology from linear to star or mesh networks). As the G' is greatly enhanced by the network topological variation, one therefore acquires a self-supporting soft solid (Fig. 4d). The gels with a high gelling capability are applied to the delivery of drugs or various benefits in personal care products.³¹⁻³²

On the other hand, one may need to prevent the gelation in some cases. Crude oil, heavy fuel, diesel fuel, etc. contain significant

proportions of higher n-alkanes, and in the cold winter, they can crystallize out and form interconnected crystal networks. The occurrence of 3% of paraffin crystal networks in crude oil can gel fuels and block the flow of liquid oils in the pipe lines or the filters in diesel engines. The effective topological modifiers may modify the topology of interconnected n-paraffin crystal networks to the linear ones, to stop gelation.³³

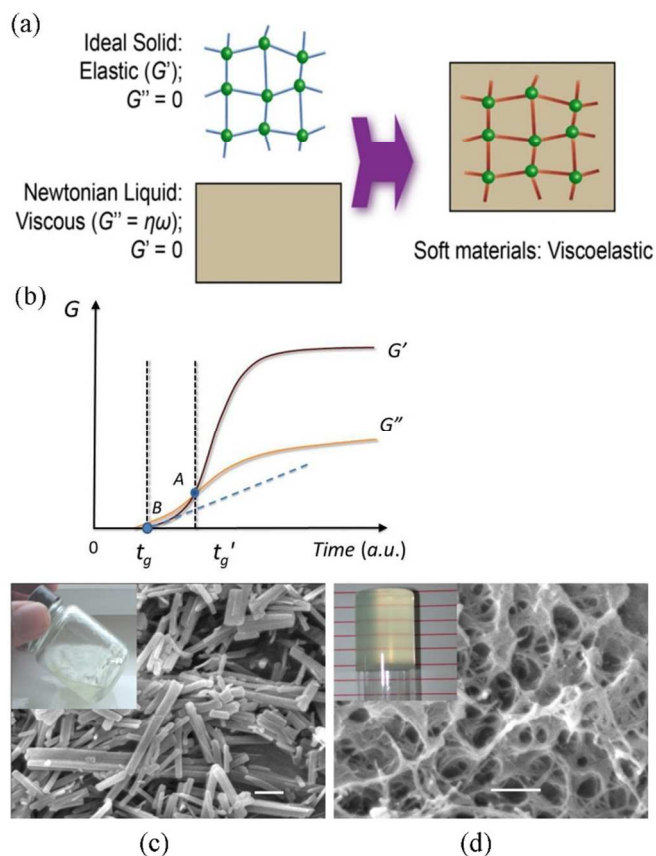


Fig. 4 (a) Schematic illustration of soft materials, and the rheological properties. (b) Definition of gelling point t_g' and t_g . (c) Separate fibers occurring in a L-DHL/DIOP system. (L-DHL: lanosta-8,24-dien-3 β -ol:24,25-dihydrolanosterol = 56:44; DIOP: di-(2-ethyl-hexyl) phthalate ($C_8H_{17}COO$)₂ C_6H_4). This system gives rise to an opaque flowing viscous liquid as shown in the picture on the right upper corner. (d) Interconnected fiber networks in a L-DHL/DIOP gel after adding 0.004wt% EVACP. The length of the bar: 1 μ m. The addition of EVACP leads to the formation of interconnected crystal networks and a clear and solid gel as shown in the picture on the right upper corner.³⁴ Scale bar: 1 μ m. Reprinted with permission from ref³⁵. Copyright 2002 American Chemical Society.

(2) Efficiency of solar cells

Apart from the rheological properties, many other macroscopic properties of materials can be altered by modifying the topology of mesoscopic structure. For instance, for Dye-sensitized Solar Cells

(DSSCs), different patterns/topologies of TiO₂ photoanodes (see Fig. 5) will give rise to different light harvesting efficiencies as listed in Table 2.³⁶ This is attributed to the fact that the networks with different topological patterns have different capabilities in harvesting photons. Obviously, the topological patterns of leaves have been evolved for millions of years to acquire the optimal light harvesting efficiency in their photosynthesis. Those TiO₂ photoanodes resemble to specific leaves may have a fast electron transport rate and good light harvesting ability, therefore give rise to a better efficiency of light harvesting of the cell devices (c.f. Fig. 5 and table 2).

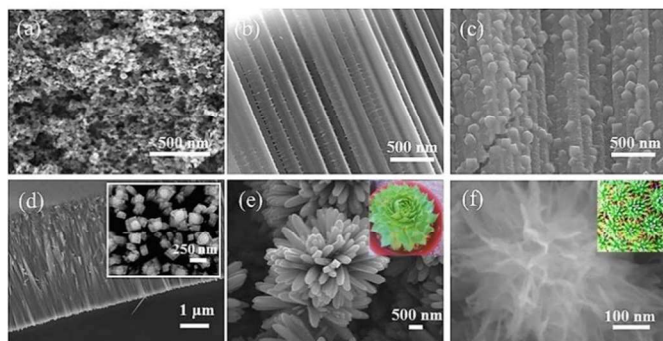


Fig. 5 SEM images of TiO₂ (a) nanoparticles, (b) smooth nanotubes, (c) heterogeneous nanotubes, (d) nanorods (inset is the top view), (e) flower-like structures, and (f) nano spherulites. Modified and reprinted with permission from Ref. ³⁶. Copyright 2011 American Chemical Society, Copyright 2013 Wiley-VCH, Copyright 2013, Royal Society of Chemistry.

Table 2 Different patterns of nano TiO₂ particles and the light harvesting efficiency of DSSC*.

Patterns	DSSC efficiency (%)
Nanoparticles	6.64
Smooth nanotubes	4.34
Heterogeneous/heterojunction nanotubes	7.24
Nanorods	3.03
Flower-like structures	4.07
Nano spherulites	8.50

*Quoted from Ref. ³⁶.

(3) Interface properties

If mesoscopic crystal networks occur on surfaces, the properties of the respective surface, i.e. surface tension, contact angle, adhesive force, etc., may be altered if the pattern or topology of crystal networks changes. For instance, the surface properties can be altered by changing the topologies/patterns of crystal networks so that they can be converted into super hydrophilic or super hydrophobic surfaces, respectively.³⁷

Zhao et. al found that the adhesive force on a super hydrophobic MnO₂ nano-structured film can be tuned by fabricating different patterns i.e. mesh-like, ball cactus-like, and tilted nanorod structures on the surface.³⁸ Table 3 summarizes the dependence of adhesive force on the patterns at a super hydrophobic MnO₂ nano-structured

film. The marvelous modulation range of the adhesive forces from 130 to nearly 0 μN endows these super hydrophobic surfaces with extraordinarily different dynamic properties of water droplets (Fig. 6; Table 3).

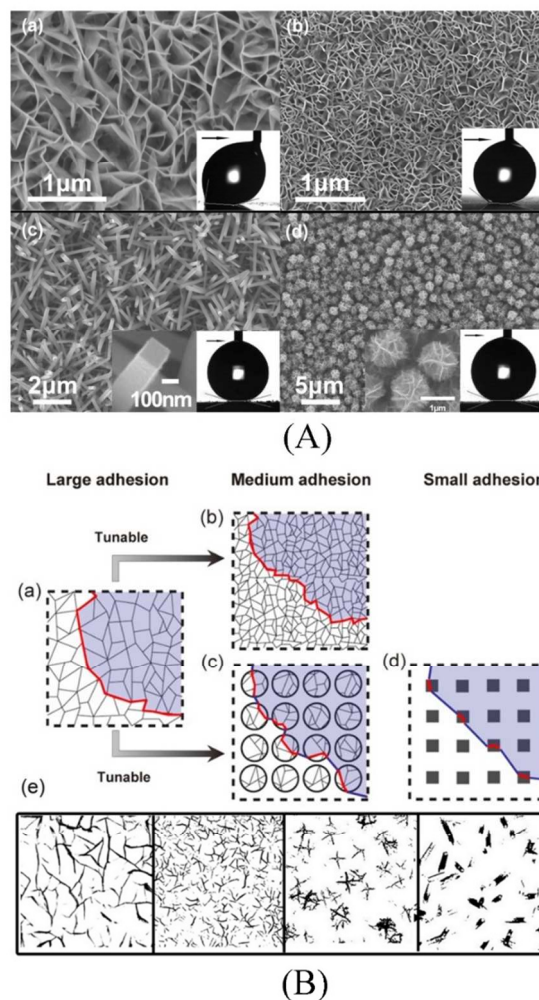


Fig. 6 (A) (a-d) SEM images of various MnO₂ patterned films: the mesh-like structure (MLS), the tilted nanorod structure (TNS), and the ball cactus-like structure (BCS) films. Insets show the dragging water droplet. The black arrow indicates the dragging direction. (a, b) MLS of a large (L-MLS) and a small mesh size (S-MLS). (c) TNS film. (d) BCS film. (B) Schematic illustration of TCL on MnO₂ films. The red lines demonstrate the possible solid-liquid-air interface contact line, and the blue lines demonstrate the liquid-air interface boundary for a droplet, respectively. (a) A continuous contact line forms on the large MLS, which exhibits a large adhesion force. (b) TCL on small MLS (S-MLS). (c) Dash-line like TCL forms on BCS. (d) A highly discontinuous dot-like TCL forms on TNS, which exhibits extremely small adhesion. (e) High contrast black and white images converted from SEM images of L-MLS, S-MLS, BCS, and TNS in (A). Reprinted with the permission from Ref. ³⁸. Copyright 2011 American Chemical Society.

From the microscopic point of view, the adhesion of patterned films depends on the way of the solid-liquid contact modes, i.e. the three-phase contact line (TCL).³⁸ The surface topology and patterns of MnO₂ films were simplified according to the high contrast black and white SEM images, shown in Fig. 6A. The solid lines describe

the possible TCL for a droplet in contact with these patterns, showing different continuity.³⁹ When a droplet is placed on most surfaces, it will spread to the equilibrium point at the local energy minimum. The contact line is pinned at a metastable state, as there will be an energy barrier for any advancing or receding of the water droplet on the surface. As for mesh-like structure (MLS) film, a continuous line-like TCL is formed on the top of nanowall sheets schemed in Fig. 6B (a). Due to the large energy barrier between the two metastable pinning states, L-MLS film generates a high contact angle (CA) hysteresis and thus a super-high adhesive force. With the decreasing of the mesh size, the energy barrier decreased as well. Consequently, the adhesive force is reduced as the mesh size shrinks (Fig. 6B (b)). Unlike the MLS structure, a highly discontinuous dot-like TCL forms on the TNS film (Fig. 6B (d)). Herein, the energy barrier between the metastable pinning states is negligible. Furthermore, an intermediate state between these two distinct TCL modes can be obtained by mixing the patterns TCL (i.e. Fig. 6B(c)). On the hierarchical BCS film, the contact line is the combination of continuous line-like and discontinuous dot-like TCL, illustrated as a separated dash-line-like TCL. Correspondingly, medium CA hysteresis and adhesive force are found on this pattern.

Table 3. Normal adhesive force and force per unit length on MnO₂ super hydrophobic surfaces with different patterns

Patterns	Adhesion (μN)
L-MLS	(13 \pm 2) '10
S-MLS	(8 \pm 1) '10
BCS	(4 \pm 1) '10
TNS	0

Notice: MLS: mesh-like structure; L-MLS, S-MLS stand for MLS with large and small mesh scale; BCS: ball cactus-like structure), and TNS: tilted nanorod structure.³⁸

2.2.2 Ordering of crystal networks

The ordering of crystallites in crystal networks exerts a direct impact on the macroscopic performance of materials. In Section 7.3, we will show in detail that the breaking stress of both spider silk and silkworm silk fibers will be greatly enhanced as the ordering of β crystallites increases.^{26, 39} In the following, we will focus more on the influence of the crystallite ordering on the hardness and mechanical strength of biominerals.

There are numerous reports concerning the influence of the ordering of biominerals on the mechanical performance.³⁷ A detailed study on the correlation between the human tooth enamel was carried by Liu *et al.*²⁷ The human tooth enamels can be roughly regarded as a bundle of nano hydroxyapatite (HAP) crystallites needles (~94%) sandwiched by some proteins and water. In human tooth enamels and the ordering of HAP crystallites, the correlation between the hardness H /elastic modulus E and the ordering of HAP crystallites was examined by small angle X-ray scattering (SAXS)⁴⁰ It follows that the ordering of biominerals varies strikingly within the dental sample: both the hardness H and the elastic modulus E increase exponentially as the ordering of the biomineral crystallites increases. (See Fig. 7).

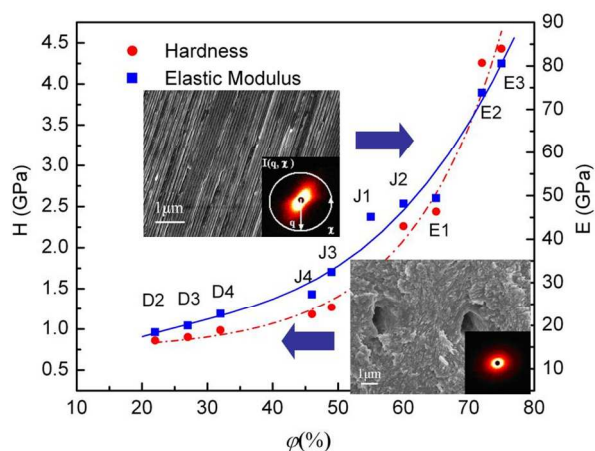


Fig. 7 The correlation between mechanical properties and the ordering of mineral crystallites within a dental sample. The hardness (H) and elastic (E) modulus vs alignment, and vs alignment. The solid circles and the hollow circles represent data measured from dental enamel and dentin, respectively. ϕ - the ordering parameter measured by small angle X-ray scattering. The complete alignment: $\phi = 100\%$, the completely disordered arrangement: $\phi = 0$. Reproduced with permission from Ref. ²⁶. Copyright 2012 Springer.

The reason behind the crystallite alignment enhanced toughness of hard tissues is not entirely clear. Nevertheless, the following so-called crack stopper model may provide some physical insight into this subject.³⁷ As indicated by Fig. 7, normally, crystals are never perfect and composed of a large number of micro crystallite grains. These grains are misfit to a small degree with respect to each other (Fig. 8a). At collision or hammering, cracks initiating at the surface of crystals can easily propagate across the crystals along the grain boundaries. This gives rise to the breakage of the crystals.

On the other hand, an entity are composed of a crystallites assembly in which lamella or needle-like nano crystallites are packed in parallel to the surface. In such a case, the grain boundaries are the head-to-tail joints of the aligned nano crystallites, which are normally terminated by the crystallites underneath. It follows then that a serious collision/hammering also causes some cracks at the surface, but are terminated by the parallel packed crystallites underneath if the collision force is not too large. (Fig. 8b). In other words, this parallel packing structure in a crystallite assembly will prevent the breakage vs the penetration of the crack lines across the crystallite assembly.

In addition to the ordered packing of HAP crystallites, the occurrence of proteins between the parallel HAP crystallites plays also a very important role in the enhancement of the structural toughness. It was found that there is a small amount of bio molecules occurring between the adjacent HAP crystallites.⁴¹ Similarly, some specific proteins are also found to be sandwiched between adjacent CaCO₃ crystallites in various seashells. These proteins serve as bio glues adhering the adjacent crystallites. As illustrated by Fig. 8c, once a crack occurs in the middle of the assembly, the neighbouring adhered crystallites will bypass the loading force through the crack and reconnect the two broken portions of the crystallites. In other words, the loading force will be redistributed from the cracked points in the three dimension, avoiding the accumulation of the force to some localized places. This obviously will enhance the breaking strength of the assembly.

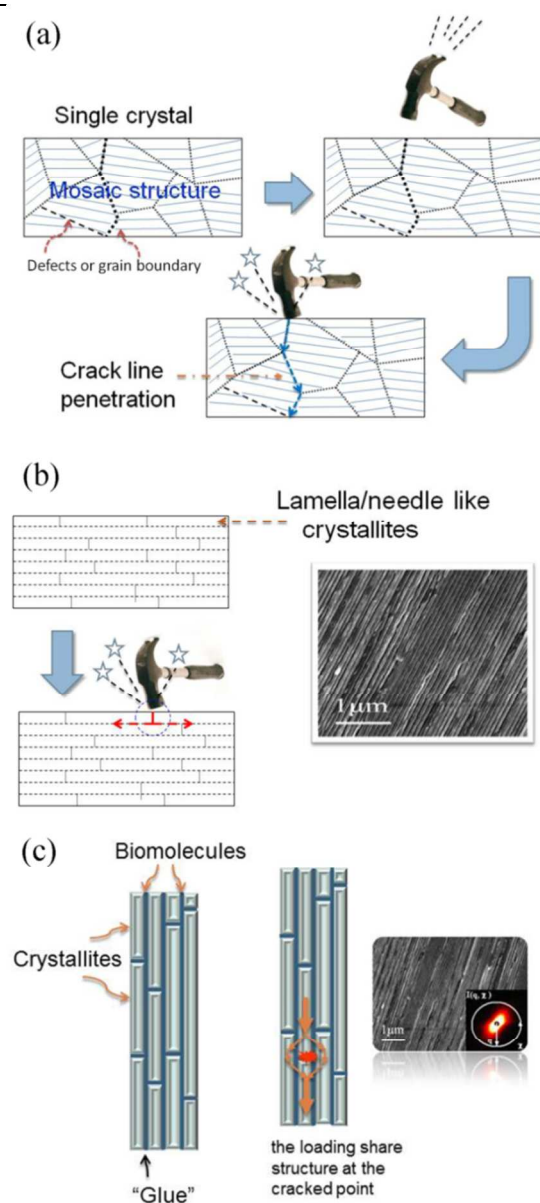


Fig. 8 The crack stopper-Parallel packing of lamella or needle-like crystals will stop the crack line to penetrate the bundled crystallites. (a) The mosaic structure of a crystal causes the propagation of crack line, leading the breakage of the crystal. Reproduced with permission from Ref. ²⁶. Copyright 2012 Springer. (b) The parallel packing of lamella or needle-like crystallites in a crystallites assembly will stop the propagation of the crack line from one crystallite to the adjacent crystallites. Reproduced with permission from Ref. ²⁶. Copyright 2012 Springer. (c) Structural enforcement by *molecular "glues"*: the proteins between the parallel HAP crystallites adhere the adjacent crystallites. Once a crack occurs in the middle of the assembly of the parallel crystallites, the neighbouring adhered crystallites will bypass the loading force through the crack and reconnect the two broken portions of the crystallites.

2.2.3 Correlation length

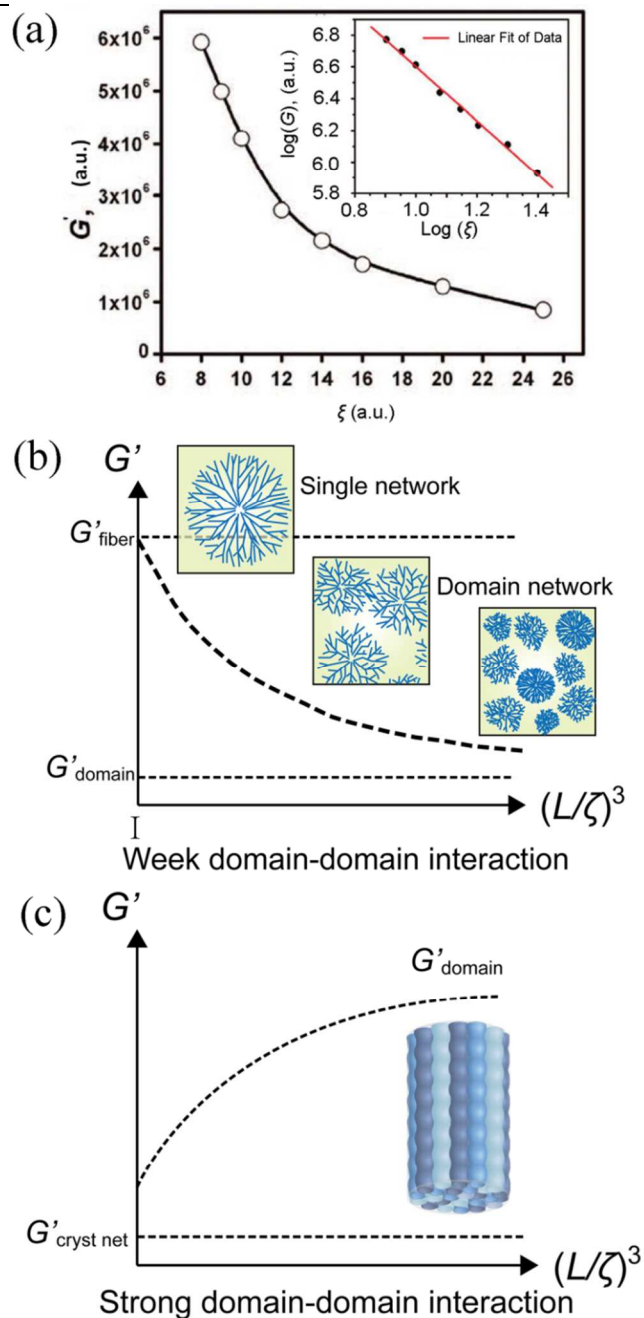


Fig. 9 Illustration of the influence of the correlation length on G' (a) The correlation length ζ on G' of gels with single fiber networks. The inset is the log-log plot of G' vs ζ . Reprinted with permission from Ref. ⁴². Copyright 2009 American Chemical Society. (b) In the case of weak domain-domain interaction, the transition of the G' of a material from $G'_{\text{cryst net}}$ to G'_{domain} as the total number $((L/\zeta)^3)$ of domains within the given system increases (L : the length of the system). Reprinted with permission from Ref. ¹³, copyright 2010, Wiley-VCH. (c) In the case of strong domain-domain interaction, the transition of the G' of a material from $G'_{\text{cryst net}}$ to G'_{domain} with the total number $((L/\zeta)^3)$ of domains within the given system.

Among the influencing factors, the correlation length ζ plays a key role in the macroscopic and physical properties of mesoscopic materials. One of the definitions refers to the average mesh size of

the crystal networks. For the Cayley tree structure illustrated in Table 1, the basic fiber length (distance between two neighbouring branching points of a fiber branch) is proportional to ζ . In general, G' decreases initially sharply as the correlation length ζ of networks increases (Fig. 9a and b). The power law $G' \sim \zeta^{-p}$ ($p = 0.5 \sim 1.7$ depending on the type of networks) holds for soft materials consisting of single networks.

In the case of materials of multi-domain fiber networks, the rheological properties are determined not only by the individual fiber networks, but also the interactions between them (the domain network). Let $G'_{\text{cryst net}}$ be the average storage modulus of individual crystal networks and G'_{domain} the storage modulus of the multi-domain network. It is expected that G'_{domain} vs the correlation length ζ of the multi-domain network follows the similar power law G'_{domain} as $\sim \zeta^r$. Although the quantitative relationship is unknown, a transition of G' from $G'_{\text{cryst net}}$ to G'_{domain} , as the total number (L/ζ)³ of domains within the given system increases is expected (L : the length of the system) (Fig. 9c). For soft materials with multi-domain networks, G' and the mechanical properties are determined synergistically by different levels of network structures. Once the average domain size reduces to the size of the fiber/crystal networks, G' and the mechanical properties will be solely determined by the fiber/crystal networks.

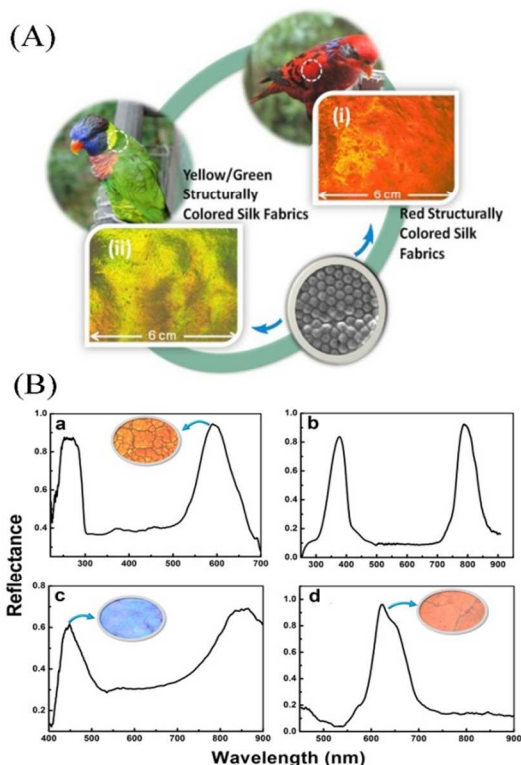


Fig. 10. (A) The creation of structural colour to silk fabrics. The two examples of silk fabrics with structural red (a) and golden (b) colours were fabricated using 240 nm and 270 nm self-assembled colloidal crystals, respectively. (B) The measured bi-structural-colour reflectance spectra. a, b, c and d are reflectance spectra for silk fibroin inverse opals fabricated by 350 nm, 450 nm, 500 nm and 700 nm colloidal spheres, respectively. The insets of a, c and d are the orange, purple and red colours observed under optical microscope for 350 nm, 500 nm and 700 nm silk fibroin inverse opals, respectively. Reprinted with permission from Ref.⁴³ copyright 2013, Wiley-VCH.

Photonic crystals are one of the materials with the periodic structure at the mesoscale.⁴³⁻⁴⁴ The reflected/refracted light interferes constructively once the wavelength is at the magnitude of the structural period. This gives rise to a specific structural colour for given photonic crystals. If the basic materials are crystalline, the periodic structure corresponds to the correlation length. Obviously, the change in the correlation length of photonic crystals gives rise to different structure colours or the reflection in the UV or IR wave ranges (Fig. 10). This demonstrates the fact that the correlation length exerts a direct impact on the specific optic performance of mesoscopic materials.

Similarly, the correlation length to a large extent determines the mechanical strength of both spider and silkworm silk fibers. More details will be given in Sec 6.3.2.

2.2.4 Strength of binding and association between structural units

How the nodes of crystal networks are linked with each other obviously determines the stability and “strength” of crystal networks. In the case of hierarchical network structures, the “strength” of the association between the “nodes”, crystal networks, of domain networks, will synergistically influence the rheological and mechanical properties of the systems.

In the case that the links in domain networks are much weaker than individual crystal networks (i.e. gels), one may expect that a much weak material. (c.f. Fig.3B-a). On the other hand, the links in domain networks are much stronger than individual crystal networks (i.e. silk fibers), one may expect that a much stronger material. (c.f. Fig.3B-c).

Once the hierarchical structures of soft materials convert a mono level structure (i.e. a sole fibrous/crystal network), one may experience a sharp change in G' of the materials. This will be reviewed in the following sections.^{6a, 45}

3. Crystallization mechanism and crystal network formation

As the basic building blocks of crystal networks are crystallites, the knowledge about crystallization is relevant for the crystal network formation. In general, crystallization consists of two major processes: nucleation and crystal growth. It can be seen from the following sessions that the kinetics of these processes governs not only the occurrence of crystals, but also the formation of crystal networks. In the following, we will present an overview on the key aspects of crystallization and discuss how the knowledge can be further extended to the field of soft materials.

As crystallization is a phase transition, the thermodynamic driving force for crystallization is subject to the chemical potential different. In other words, crystallization occurs because the chemical potential μ_i^{ambient} of a growth unit in the ambient mother phase is higher than the chemical potential μ_{crystal} in a crystal phase. The difference between the chemical potentials μ_i^{ambient} and μ_{crystal} is given by:

$$\Delta\mu = \mu_i^{\text{ambient}} - \mu_{\text{crystal}} \quad (1)$$

(Subscript i denotes the solute in the ambient phase.) In solutions, the chemical potential of species i is given by^{2, 22}

$$\mu_i = \mu_i^0 + k_B T \ln a_i \approx \mu_i^0 + k_B T \ln C_i \quad (2)$$

where a_i denotes the activity of species i which is often approximated by concentration C_i . μ_i^0 denotes the chemical

potential of species i in a standard state ($a_i = 1$). With Eq. (3), the thermodynamic driving force for crystallization is given by:

$$\frac{\Delta\mu}{k_B T} = \ln \frac{a_i}{a_i^{eq}} \approx \ln \frac{C_i}{C_i^{eq}} \quad (3)$$

(a_i^{eq} , C_i^{eq} are, respectively, the equilibrium activity and concentration of species i .) Given the definition of the supersaturation s for crystallization²²

$$\sigma = (a_i - a_i^{eq})/a_i^{eq} \approx (C_i - C_i^{eq})/C_i^{eq} \quad (4)$$

Eq. (4) can be simplified as

$$\Delta\mu/k_B T = \ln(1 + \sigma) \cong \sigma \quad (\text{in the case of } \sigma \ll 1) \quad (5)$$

In case $\Delta\mu > 0$, the system is said to be supersaturated and nucleation and crystal growth are thermodynamically expected. Conversely, when $\Delta\mu < 0$, the system is under-saturated and crystals will dissolve. For $\Delta\mu = 0$, the ambient phase is in equilibrium with the crystalline phase.

3.1 Nucleation: the initial and one of the most important processes in crystallization

Nucleation, as one of the most crucial steps, determines whether and which crystalline phase occurs in the case of polymorphism, the size and size distribution of crystalline particles, and more importantly the formation of crystal networks or hybrid materials.¹³

Since the nucleation phenomenon was identified and studied by Gibbs,^{46a} numerous models and theories have been published. Nevertheless, the first detailed experiment monitoring the nucleation process from the pre-nucleation to post nucleation stages and quantitatively comparing them with the theories was carried out by Liu et al. using colloidal particles driven by an alternating electric field. It follows that constituent particles in solutions on collision, join into groups of two, three, four, or more particles, forming dimers, trimers, tetramers, etc., overcoming a nucleation barrier and growing into crystals.

A characteristic feature of the nucleation process is that the substance with the properties of the new phase is fluctuating and localized in small spatial regions.^{23, 44a, 47} These regions are occupied by various numbers of atoms, molecules in the form of clusters. The clusters remaining at equilibrium with the surrounding mother phase are the critical nuclei, and the smaller or the larger clusters are the subnuclei or supernuclei, respectively. Only the supernuclei are the clusters that can grow spontaneously to reach macroscopic sizes. For simplicity, we call hereafter the subnuclei “clusters”, and the supernuclei “nuclei”. The occurrence of the nucleation barrier is attributed to the occurrence of the interface (or surface) free energy between the newly created phase and the ambient phase, which gives rise to the following two opposite effects in a supersaturated ambient phase:

(1) As the crystalline phase is a stable phase, the emergence of the new phase from the ambient phase reduces the (Gibbs) free energy of the system.

(2) The increase in the size of the crystalline new phase increases the interface (or surface) area, and consequently the interface (or surface) free energy γ . This enhances the Gibbs free energy of the system.

The combination of the two opposite effects gives rise to the so-called nucleation barrier ΔG^* , at $r = r_c$, or $n = n^*$. The spherical

cluster of n^* molecules is the critical nucleus, r_c is the radius of curvature of the critical nuclei,^{23, 44a, 47}

$$\Delta G^* = \frac{16\pi\gamma^3}{3(\rho_c\Delta\mu)^2} \quad \text{and} \quad r_c = \frac{2\gamma}{\rho_c\Delta\mu} \quad (6)$$

where ρ_c is the particle number density in nuclei and γ is the surface free energy area density, ΔG^* and r_c are the so-called nucleation barrier and the critical size, respectively. The nucleation barrier is the Gibbs free energy barrier to be overcome in order to form a stable crystalline phase. As shown by Fig. 11a, crystalline clusters are thermodynamically unstable until they reach the critical size r_c . Obviously, the nucleation rate depends on the nucleation barrier. The lower the nucleation barrier, the higher the nucleation rate. Both ΔG^* and r_c are the driving force and the interface (or surface) free energy γ dependent.

In the aforementioned process, as the probability of nucleation is uniform throughout the whole system, it is therefore known as homogeneous nucleation.^{46, 48} We notice that in most cases, homogeneous nucleation is difficult to take place due to the very high nucleation barrier (Fig. 11c). It was found recently that the genuine homogeneous nucleation of ice never happens even at the temperature below -40°C .⁴⁰ This is subject to the very high interfacial free energy between ice and water. Nevertheless, any natural process can always find its easiest path to proceed. Two of the most common ways to bypass the high nucleation barrier of homogeneous nucleation is (i) heterogeneous nucleation; and (ii) multistep (two step) nucleation/crystallization.

Heterogeneous nucleation occurs when foreign bodies/substrates are present in the system. The stronger interactions between the nucleating phase and the substrates can compensate for the total free energy increase resulting from the rise of the interfacial energy of nucleating clusters (Fig. 11a). Therefore, the occurrence of foreign bodies will lower the nucleation barrier (Fig. 11c). In such cases, the probability of nucleation in the adjacent regions of the foreign bodies is then higher than elsewhere in the system. This is why it refers to heterogeneous nucleation.

The effect of foreign bodies in lowering the nucleation barrier can be quantified by an interfacial correlation factor $f(m)$ which is defined as:

$$f(m) = \frac{1}{4}(2 - 3m + m^3) \quad (7)$$

where ΔG^*_{homo} is the homogeneous nucleation barrier as defined by Eq. (9) and $\Delta G^*_{\text{hetero}}$ is the heterogeneous nucleation barrier. $f(m)$ indicates how much the nucleation barrier is reduced with respect to ΔG^*_{homo} due to the occurrence of foreign bodies/substrates. The parameter m describes the structural match between the nucleating phase and the substrate. For a flat substrate, one has^{18g, 48a, 49}

$$f(m) = \frac{1}{4}(2 - 3m + m^3) \quad (8)$$

with

$$m = (\gamma_{\text{sf}} - \gamma_{\text{sc}})/\gamma_{\text{cf}} \approx \cos\theta \quad (-1 \leq m \leq 1) \quad (9)$$

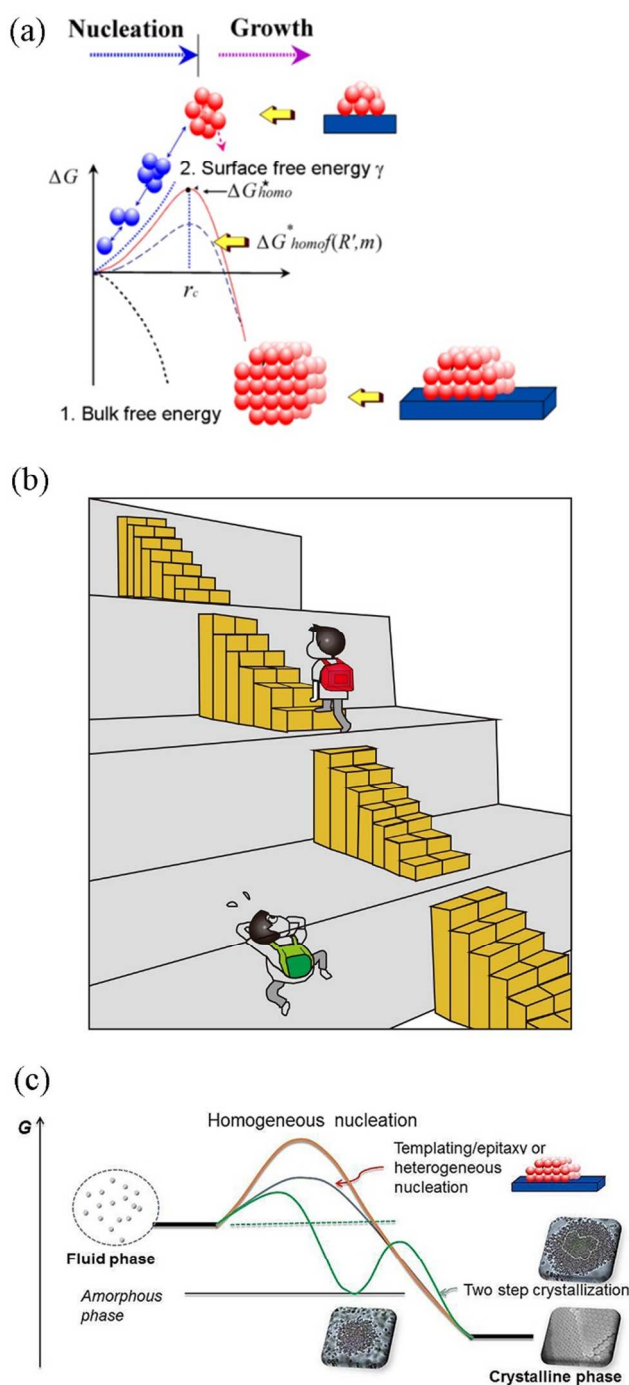


Fig. 11 (a) Crystallization normally takes place via nucleation, followed by the growth of crystals. Nucleation is a kinetic process of overcoming the nucleation barrier, which is the outcome of the occurrence of the surface free energy γ . (b) If a barrier is too high, nature can always find a multiple step path of lower barriers to bypass the single step process. (c) For the nucleation on a substrate or the multiple step crystallization where an intermediate phase is inset, a high energy barrier is replaced by one or several much lower energy barriers. This speeds up the kinetic process. Parts of images reprinted with permission from Ref. ⁵⁰. Copyright 2007 American Chemical Society.

where θ is the contact angle of the nucleus on the substrate, γ_{sf} and γ_{sc} are surface free energy between the substrate and fluid phase, substrate and crystal phase, respectively. In case of a perfect match, $\gamma_{\text{sc}} \rightarrow 0$ and $m \rightarrow \gamma_{\text{sf}}/\gamma_{\text{cf}}$. In the case of a perfect match, $\gamma_{\text{sc}} \rightarrow 0$ and $m \rightarrow \gamma_{\text{sf}}/\gamma_{\text{cf}}$. In the case of a perfect match, $\gamma_{\text{sc}} \rightarrow 0$ and $m \rightarrow \gamma_{\text{sf}}/\gamma_{\text{cf}}$. This implies that the heterogeneous nucleation barrier vanishes almost completely when the nucleating crystal is well ordered and oriented with respect to the structure of the substrate. As the structural match changes from a perfect match to a poor match, m decreases from 1 to -1. When $m \rightarrow -1$ ($f(m) \rightarrow 1$), there is no correlation between the substrate and the nucleating phase. In this case, the substrate almost exerts no influence on nucleation kinetics, which is equivalent to homogeneous nucleation. Nuclei emerging in this case are completely disordered, bearing no correlation to substrate. In general, for a certain system, m is between -1 and 1, which means the primary nucleation is normally governed by heterogeneous nucleation. Nucleation kinetics can be described by nucleation rate^{46d, 48b, 51}, which is defined as the number of mature nuclei created per unit volume-time from the system. There are two states of nucleation we encounter frequently: one is the stationary state and the other is non-stationary state. The stationary state is one of the most relevant states, which corresponds to the state where the cluster size distribution does not change with time. This is a state which happens only in a certain period of a nucleation process.

Taking into account the effect of substrates on both the nucleation barrier and the transport process, the nucleation rate is given by^{46d, 51a, 52}

$$J = f''(m)[f(m)]^{1/2} \times B \exp\left[-\frac{16\pi\gamma_{\text{cf}}^3\Omega^2}{3kT[kT\ln(1+\sigma)]^2} f(m)\right] \quad (9)$$

and

$$f''(m) = \frac{1}{2}(1-m) \quad (10)$$

where B is the kinetic constant. In the case of homogeneous nucleation, the growth units can be incorporated into the nuclei from all directions. However, in the case of heterogeneous nucleation, the presence of a substrate will block the collision path of the growth units to the surfaces of these nuclei from the side of the substrate. This is comparable to a “shadow” cast on the surface of nuclei.^{18g, 48a, 49, 53} The “shadow” effect of substrates is described by $f''(m)$ in the pre-exponential factor, which is the ratio between the average effective collision in the presence of substrates and that of homogeneous nucleation (i.e., in the absence of a substrate).

Note that for homogeneous nucleation, one has $f''(m) = f(m) = 1$. In this case, Eq. (9) is converted to^{22a}

$$J = B \exp\left[-\frac{16\pi\gamma_{\text{cf}}^3\Omega^2}{3kT[kT\ln(1+\sigma)]^2}\right] \quad (11)$$

In practice, nucleation will transit from “zero” to the stationary state, and gradually reach the completion (zero). The transition states are non-stationary.

The multistep (two-step) nucleation/crystallization is another pathway to reduce the nucleation barrier. The formation of crystal nuclei from liquid is sub-divided by two steps of transition: the transition from an initial (i.e. solution) to an intermediate phase (i.e. a concentrated solution/amorphous phase or a less stable crystalline phase) occurs first. The crystalline nuclei subsequently occurs from the amorphous droplets.^{46d, 50} The occurrence of the metastable

amorphous phase can greatly reduce the nucleation barrier and enhance the nucleation of crystals (Fig. 11b & c). This is due to the fact that the intermedium phase is much closer to the initial phase in terms of structure and properties. This causes a much lower interfacial energy, consequently a much lower nucleation barrier. The same holds for the transition between the intermedium phase and the final crystalline phase. It is so to say that it would be much easier to replace a big step by two or more much smaller steps (the principle of the *Ostwald Step Rule*, c.f. Fig. 11b).⁵⁴

Recently, it was suggested that two-step crystallization (TSC) may be a mechanism underlying most crystallization in typical atomic systems.⁵⁰ We notice that the first quantitative measurement of TSC at single-particle level was achieved in the AEF-controlled two-dimensional (2D) colloidal system.^{46c, 50} Experimentally, two step nucleation is often found in biomineralization or macromolecular crystallization.^{46c} It normally occurs when the nucleation process experiences some difficulty.⁵⁵ Biomineralization is the process by which organisms form a variety of functional crystalline structures. An intriguing feature of these functional crystalline materials is their well-defined size and shape.⁵⁶ It is believed that the amorphous metastable phases in biomineralization not only reduce the nucleation barrier but also plays a key in precisely controlling the shape and the size of crystalline structures.⁵⁷

As to be shown in the following sessions, the formation of crystal networks to a large extent is governed by nucleation. Self epitaxial nucleation and Supersaturation Driven Interfacial Structure Mismatch Nucleation Or *crystallographic mismatch* (or *noncrystallographic*) branching or is in fact a type of heterogeneous nucleation, where the substrates and the nucleating phase belong to the same type of materials.

Furthermore, two-step nucleation also plays a key role in the formation of some specific patterns of crystal networks. As discussed before, the two-step nucleation is an effective way to bypass a high nucleation barrier by surpassing two much lower barriers. It has been found that the occurrence of numerous crystal networks is attributed to the high nucleation barrier of crystallization. It follows that the formation of these crystal networks often take place via two step crystallization.^{46c, 46d} Fig. 12 shows the formation of hydroxyapatite (HAP) spherulitic patterns via two step crystallization. It shows from very recent research that in a simulated body fluid solution, some amorphous calcium phosphate (ACP) aggregate spheres occur first in the solutions.⁵⁸ This is followed by the transformation from ACP aggregate spheres to HAP spherulites (HAP crystal networks). In this process, the nucleation of ACP spheres is much easier and occurs first due to the much lower nucleation barrier. The ACP spheres will then serve as templates to promote the nucleation and growth of HAP crystals (Heterogenous nucleation). This whole process of the two step crystallization and the HAP spherulitic pattern formation is demonstrated clearly by Fig. 12. It follows that the ACP cores are found in the centers and the HAP crystallites occur as the radial arms initiating from the centers of spherulites.

We notice that both heterogeneous nucleation and two-step nucleation/crystallization are to lower the kinetic barrier of crystallization. The consequence of these two types of nucleation paths often leads to the formation of a variety of different patterns of crystal networks. In other words, the formation of crystal networks is the kinetically favoured option.

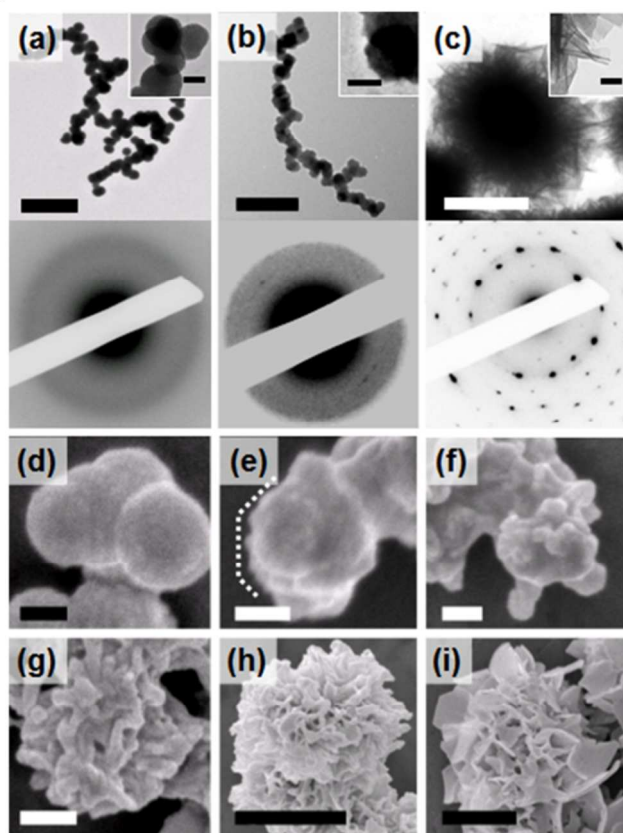


Fig. 12 The multi-step crystallization of calcium phosphate phases. The phase and morphology evolution of calcium phosphate minerals: (a-c) TEM images and SAED patterns of the precipitates. (a) Initial formed amorphous calcium phosphate (ACP) spheres. Bar: 1 μm and 100 nm. (b) Intermediate state of ACP. Bar: 1 μm and 100 nm. (c) Final hydroxyapatite (HAP) spherulite. Bar: 1 μm and 200 nm. (d-i) SEM images of the evolution of ACP. (d) 3 min. (e-g) 67-73 min. (h) 90 min. (i) 7 hr. Bar: (d-f) 100 nm; (g) 200 nm; (h-i) 1 μm . Reprinted with permission from Ref. ⁵⁸. Copyright 2010 Royal Society of Chemistry.

3.2 Crystal Growth

The size and shape of crystallites is to a large extent controlled by the growth of the crystallites. In general, the growth of crystals can be regarded as a process of delivering growth units from the bulk to the crystal surface and incorporating these units into the kinks. In the case of faceted growth, the crystal surface is atomically smooth and the kinks occur only at the steps on the crystal surface. In this case, the steps can be regarded as “sinks” for growth units to enter the crystals.^{49b} Each advancing step disappears when it spreads over the surface and reaches the edge of the surface. In order to continue the growth of the crystal surface, a subsequent crystal layer needs to be generated on the existing crystal surface. Therefore, the step source for the creation of new layers determines the growth rate of the crystal surface. Due to the presence of the step free energy, the creation of a new layer on the existing layer of the crystal surface requires overcoming a free energy barrier, the so-called 2D nucleation barrier.^{22a, 51c} Normally, for the growth of flat or faceted crystal surfaces, the screw dislocations occurring on the surface provides uninterrupted step sources for a layer-by-layer growth, and in such cases the growth is controlled by screw dislocation mechanism.^{22a, 59}

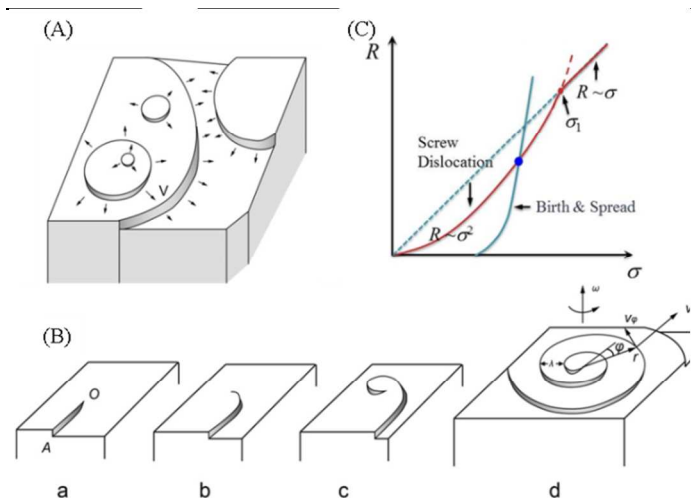


Fig. 13 Illustration of the (A) the Birth-and-Spread model. The model assumes (1) There is no intergrowth between 2D nuclei; (2) The lateral spreading velocity V^* is constant, independent of the island size; (3) Nuclei can be born anywhere, around nucleating particles, which can occur on incomplete layers as well as on islands; (B) the Screw dislocation model of nucleation and growth of crystals. (a)-(d) of (B) show the process of crystal growth through the screw dislocation model; (C) the supersaturation dependence of crystal growth rate through the two models. Here, we will review the two most commonly encountered 2D nucleation growth mechanisms: the Birth-and-Spread mechanism and the Screw Dislocation mechanism.

(1) *The Birth-and-Spread mechanism.* This is the commonly adopted model in the case of the growth of dislocation free crystal faces (Fig. 13A). The key assumptions of the Birth-and-Spread model are summarized in the caption of Fig. 13A. Once crystals are perfect and defect free, the growth of crystal faces is governed by two 2D nucleation growth mechanism.^{51c} This implies that the crystal faces grow by depositing new crystal layers on the top of the existing layer by 2D nucleation. The continuous deposition of new layers leads to the advance of the crystal face in a given orientation. It follows that the crystal growth rate can be given by

$$R = C_1(\sigma)^{5/6} \exp\left\{-\frac{\Omega\gamma_{\text{step}}^2 h\pi}{3k^2 T^2 \times \ln(1+\sigma)}\right\} \quad (12)$$

In case $\sigma \gg 1$,

$$R \sim C_1(\sigma)^{2/3} [\ln(1+\sigma)]^{1/6} \sim \sigma \quad (13)$$

(2) *Screw Dislocation Mechanism* (BCF, Chernov models).

Normally, to maintain the dislocation free growth of crystals is not easy. In many cases, the growth of crystals is governed by other mechanisms, i.e. the Screw Dislocation mechanism. The concept of growth spiral was developed by Frank⁶⁰ and the mathematical spiral growth theory was developed later by Burton et al.⁶¹ The BCF theory provided an enormous breakthrough in the science of crystal growth.⁶² As first noticed by Frank in 1949, a step emerging from the point where a screw dislocation crosses the surface cannot disappear in the course of growth, since a crystal with a screw dislocation actually consists of a single atomic plane rolled into a helicoid (Fig. 13B). Therefore, a dislocation outcrop is a continuous acting layer source which eliminates the need for 2D nucleation in order to continue the growth of a singular face. As shown by Fig.

13B, step OA (Fig. 13 B (a)) is straight at the initial stage. In the course of growth the step starts moving to the right; since the linear velocities of its various parts are the same, their angular velocities decrease with the distance from O. Therefore the step shape will change until the step turns into a spiral which ensures constancy in the angular velocity of the “rotation” of all the parts of the step about point O (Fig. 13B(b-d)). According to BCF, When supersaturation is relatively small ($\sigma \ll \sigma_1$) one has the growth rate of crystal faces

$$R \cong A\sigma_1^2 \quad (14)$$

With

$$\sigma_1 = 2\pi\Omega\gamma_{\text{cf}} / (kT\lambda_s) \quad (15)$$

where A is a kinetic coefficient, λ_s denotes the surface diffusion length of growth units. This is the so-called parabolic law of spiral growth. In the case that supersaturation is relatively large, $\sigma \gg \sigma_1$, one has then

$$R \cong A'\sigma \quad (A' = A\sigma_1) \quad (16)$$

Normally, each of the above mechanisms governs the growth of crystals in different regimes. For the bulk crystal growth, the spiral growth mechanism is kinetically favoured at relatively low supersaturations, as under this situation, no 2D nucleation is required to generate a new crystal layer. On the other hand, the birth and spread mechanism is more kinetically favoured at high supersaturations as the 2D nucleation barrier becomes much lower, and the source of new layer creation won't be limited by the density of screw dislocation points (Fig. 13C). For the growth of tiny or needle like crystals, spiral dislocation will destabilize the crystallites, the growth of the tips is then governed by the birth and spread mechanism or the rough growth mode. In the case of rough face growth, as the stage of step creation is absent, the growth rate of the faces is normally higher than the flat faces. Consequently, they will be absent from the morphology of crystals.⁶³ We notice that in the case of small molecular gels, the networks are mainly branched crystalline needles/fibers. As the tips are tiny and experience higher supersaturations, the growth of the crystalline needles/fibers is then controlled by the birth and spread mechanism or the rough growth mode.

4. Crystal network formation: assembly pathways and controlling mechanism

As mentioned, the hierarchical structures of crystal networks and domain networks determine the properties/performance of soft materials. Then the key question to be addressed is how crystalline fibers/crystallites are linked with each other (or “crystallites networking”). In this regard, the kinetics will be discussed as follows.

4.1 Crystal network: the assembly of crystallites

Evidentially, the pathway of crystal network formation is very crucial. The knowledge acquired can be applied to identify effective approaches in engineering the crystal networks of meso materials. We notice that although we have discussed in the previous sections some of the ways of the formation of crystal networks, i.e. HAP spherulites, an overview on the various mechanisms of crystal

network assembly is needed. Herewith we will summarize the typical pathways of crystal network assembly as follows.

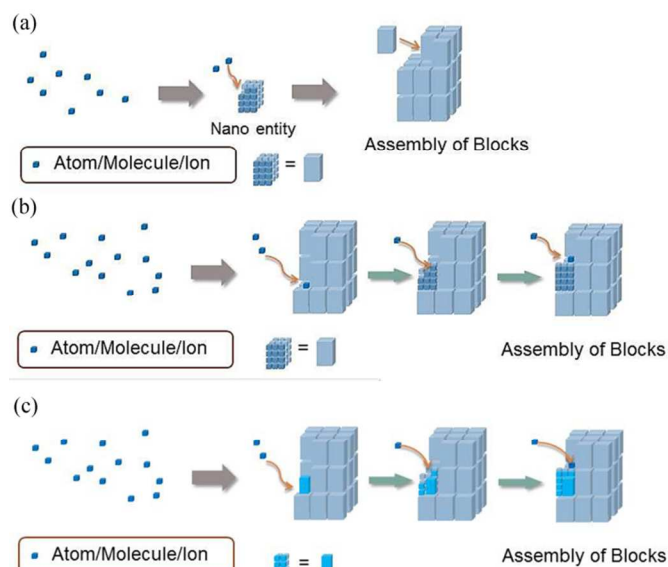


Fig. 14 Schematic illustration of two typical pathways of crystal network assembly: (a) Two-step process of assembly; (b) One step process of assembly; (c) Mixed mode of assembly.

(1) Two-step process of assembly

The two step process of crystal network assembly is illustrated by Fig. 14a. In such a process, atoms or molecules are assembled via nucleation and growth into nano crystals first. These nano crystals/blocks will be further assembled into crystal networks.

Notice that the assembly of nano crystallites into crystal networks is difficult and turns out to be the key step. We notice that the assembly of crystallites are referred by Cölfen and co-workers as “meso crystals”.⁶⁴ Nevertheless, they are a sort of colloidal crystals. Fig. 15A shows typical polystyrene spheres (PS) colloidal crystals.^{46d} Although PS spheres are not nano crystals, the way they are assembled into colloidal crystals is similar to what is described by the second step in Fig. 14a.^{44a, 46c, 50} Notice that in addition to the traditional colloidal interactions, the long range ordering the colloidal crystals acquired might be attributed to the super-long range interaction between nano crystallites. In this regard, the initiation of the key step (second step) of “meso” (or colloidal) crystals is still via nucleation, which has been verified experimentally by colloidal spheres crystallization (Fig. 14A).^{26, 44a, 46d}

As another example, Li *et al.* applied the *in-situ* high-resolution TEM to illustrate the kinetics of multistep structural transformation (Fig. 15B)⁶⁵. It follows that a nanocrystal starts to move towards the surface of the parent crystal followed by its rotation and local adjustment until both nanocrystals align reasonably well.

Recently, Bian *et al.* summarized the formation of the binary mesocrystallization of metal oxide via the *two-step process of assembly*. This will give rise to a) mesocrystals containing a single metal oxide, b) binary mesocrystals, where each nanocrystalline subunit contains one of the pure metal oxides, c) solid solution meso-crystals, where each nanocrystal contains both metal oxides.⁶⁶

We notice that the assembly of crystallites in an ordered manner will become increasingly difficult as the size of crystallites increases. This is due to the fact that structural complexity of multiple crystallite assembly will increase and the structural match requirement will be difficult to meet as the crystal size increases. Therefore, the

two step process of crystal assembly occurs normally at the nano or meso scale. On the other hand, the Brownian Motion at the nanoscale which deteriorates the structural alignment of tiny crystallites is relatively severe at room temperature. Therefore, the media capable of suppressing the random motion of crystalline particulates may facilitate this process.

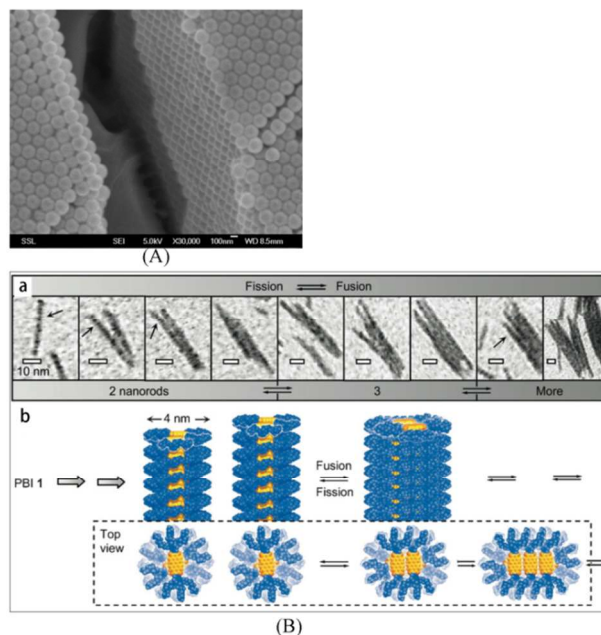


Fig. 15 Examples of the two step process of assembly as illustrated by Fig. 14a. (A) Self assembled colloidal crystals. Reprinted with permission from Ref. ²⁶. Copyright 2014 Springer. (B) Cryo-TEM images of the lateral fusion process of the adjacent nanofibers into nanosheet-like crystals. Reprinted with permission from Ref. ⁶⁵. Copyright 2010 Wiley-VCH.

(2) One-step process of assembly

The so-called one step process is illustrated by Fig. 14b. It follows that atoms or molecules are directly engaged in the formation of crystal networks. This implies that the crystallization and the crystal network formation take place simultaneously. The formation of each crystal block in the networks is then controlled by the nucleation and growth of crystallites. The nucleation and growth of daughter crystallites are influenced directly by the mother crystals. The orientation of the newly formed crystallites will be largely controlled by the “fields” of parent crystallites or crystal networks. In comparison with the two step processes, as the crystalline blocks can grow from a very small size without jeopardizing the structural correlation between the crystallites, the crystal assembly can be very strong and sufficiently large in size.

Fig. 16 displays the ordered assembly of hydroxyapatite (HAP) crystallites in simulated body fluids with 1mM fluoride ion (F⁻).⁶⁷ Fig. 16a illustrates the process how the HAP crystallite assembly occurs and Fig. 16(b-c) shows the state of the ordered HAP crystallite assembly. These are identical to the one step process as illustrated by Fig. 14b.

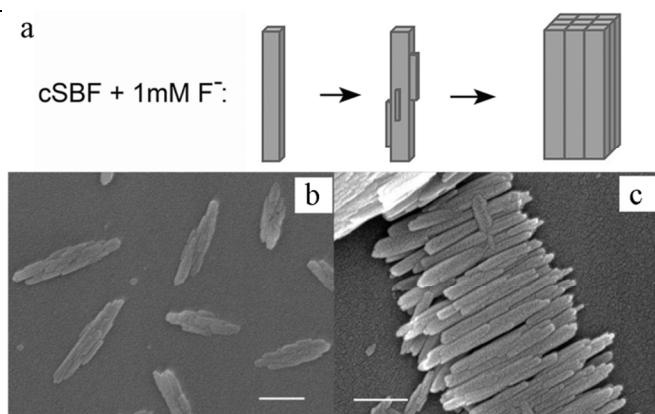


Fig. 16. (a) Illustration of the assembly of hydroxyapatite; (b) and (c) compact and ordered assembly of rod-like crystallites obtained at relatively low supersaturations in regime II; Scale bars: 200 nm. Reprinted with permission from Ref. ⁶⁷. Copyright 2009, American Chemical Society.

(3) Mixed mode of assembly

In most cases, the formation of crystal networks can be the combination of the aforementioned two processes. As nano sized crystallites are easy to acquire structural match with the parent crystals, they are adsorbed onto the parent crystals first with a proper structural alignment (*two-step process*). It follows by the further growth of the adsorbed daughter crystals via the continuous incorporation of atoms or molecules under the influence of the parent crystals/crystal networks (*one step process*) (see Fig. 14c).

(4) Foreign molecule mediated assembly

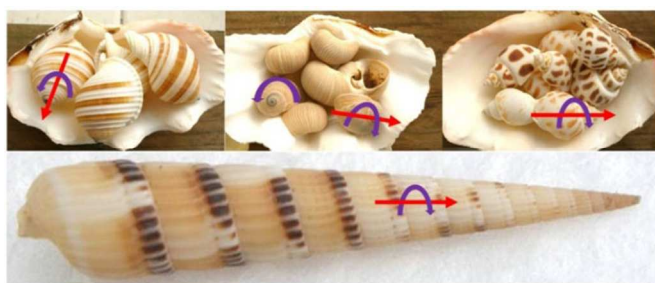


Fig. 17 General gastropod species have right-handed shells. Reprinted with permission from Ref. ⁶⁸. Copyright 2013, Royal Society of Chemistry.

The ordered assembly of crystallites are often regulated or facilitated by some particular foreign molecules. These molecules not only promote but guide the specific way of assembly. We notice that although CaCO_3 or hydroxyapatite (HAP). Crystals are very regular, the crystallites can be constructed in a variety of patterns by bio molecules (Fig. 17-18). Notice that foreign molecules can facilitate either the two step or the one step processes. On the other hand, the foreign molecular mediated assembly is often observed in a very similar way as demonstrated by the one step process. For instance, in biomineralization, some macro and small organic molecules generated from gene expression usually assemble into ordered templates to control mineral precipitations.^{41b, 41c} In particular, many artificial amphiphilic molecules or even crystals can form a variety of dispersed hierarchical structures or templates.⁵⁸ Fig. 18 demonstrates an example of molecular guided construction of nano helices: Two kinds of chiral organic-inorganic nano helices (L- and R-enantiomers) spontaneously formed and each individual helix

can even be proliferated to a relative large material complex with homochiral characteristics. In this case, bis-(2-ethylhexyl) sulfosuccinate sodium salt (AOT) and bovine serum albumin (BSA) were adopted as the models for biological amphiphilic and macro molecules, respectively. AOT is an asymmetric, double-chained amphiphilic molecule. They can assemble into various mesomorphous phase, which have been widely used in biomimetic crystallization.⁶⁸ The synergistic effect of AOT and BSA on CaP mineralization gave rise to a nano helix formation (Fig. 18(a-b)), which was not observed in the use of AOT and BSA separately in the same calcium phosphate mineralization system, respectively. Therefore, the helix structure formation was attributed to the coexistence of AOT, BSA and CaP.

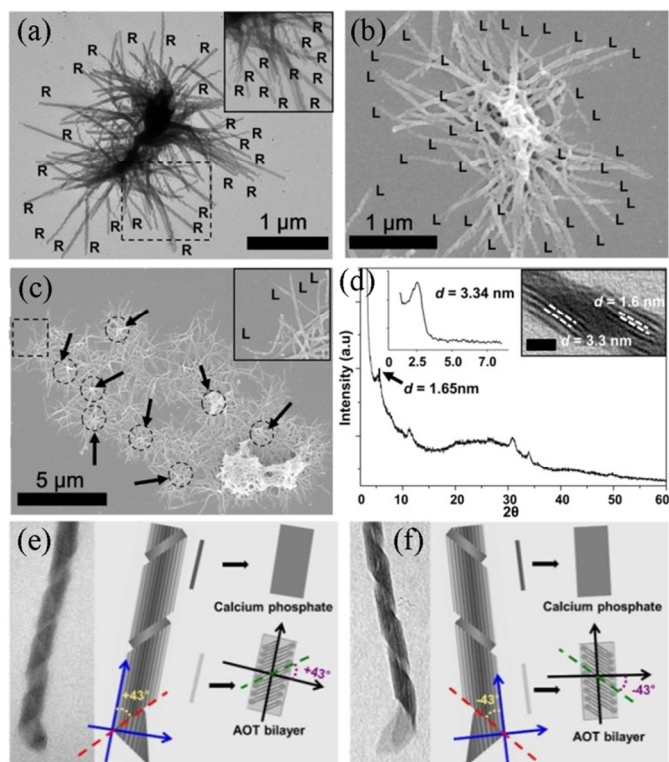


Fig. 18 Molecular guided construction of nanohelices. Organic molecules regulating the architecture of biominerals in a bio mineralization system of a racemic mixture of chiral amphiphile (bis-(2-ethylhexyl) sulfosuccinate sodium salt, AOT) and bovine serum albumin (BSA) in supersaturated calcium phosphate (CaP) solutions. a) Homochiral cluster consisted of R-helices exclusively. b) Homochiral cluster consisted of L-helices exclusively. c) Homochiral helix networks; circles indicate the cluster centers in the net; insert was a magnification of the rectangular region, showing the spiral details of the L-enantiomers. d) Small Angle X-Ray Scattering (SAXS) and Wide Angle X-Ray Scattering (WAXS) patterns of the helices. $d = 3.34$ nm and $d = 1.65$ nm represented the first and the second diffractions of the lamellar structure in the helices, respectively. The insert TEM image showed each organic (light line)-inorganic (dark line) unit had a uniform width of 3.3 nm and the dimension of an AOT bilayer was 1.6 nm (bar=10 nm). e) and f) TEM and schemes of the L- and R- helix. Reprinted with permission from Ref. ⁶⁸. Copyright 2013 Royal Society of Chemistry.

We notice that the resulted helices further developed into micron-sized clusters. Among each cluster, the nano helices extended radially outward from a core. Furthermore, some clusters connected with each other to form a network (Fig. 18). As the basic building

blocks, the helices were chiral and had two kinds of spiral enantiomers, L- and R-forms. Although the overall amounts of the L- and R-helices in the reaction system were equal, only one helix enantiomer could be identified within a cluster or network. This suggests that a chiral recognition or separation occurred during the cluster and network generation.

4.2 Ordered versus disordered assembly

Normally, the assembly of crystallites refers to the packing of crystallites with a certain degree of ordering or symmetry while aggregation denotes the disordered packing (Fig. 19a).

Nevertheless, the so-called *assembly* and *aggregation (or disordered assembly)* can be interchanged under different conditions. Here the conditions and the mechanisms governing the formation of assembly and aggregation will be summarized.

Notice that the inter transformation of the ordered and disordered assembly of crystal networks may also occur via the one-step and the combined processes of assembly. Under such conditions, a number of crystallites growing together via self-epitaxial nucleation and growth should give rise to the ordered assembly. Nevertheless, with the influence of the perturbation of external conditions, the crystallographic alignment between adjacent crystallites may be lost, leading to crystallographic mismatch assembly or structural misalignment of crystal networks. This process is referred to crystallographic mismatch nucleation mediated branching of crystal networks.^{18c, 35, 41a, 69} Based on the nature of perturbation, one normally has the following three types of mismatch nucleation mediated branching stimulating approaches:

(1) *Supersaturation driven interfacial structural mismatch nucleation mediated assembly/branching.* This mismatch assembly is caused by an abrupt increase in supersaturation/supercooling. More details are given below.

(2) *Additives driven interfacial structural mismatch nucleation mediated assembly/branching.* The additives include polymers, surfactants, small molecules and particulates etc.

(3) *External fields interfacial structural mismatch nucleation mediated assembly/branching.* The external fields include ultrasound, electric field, etc.

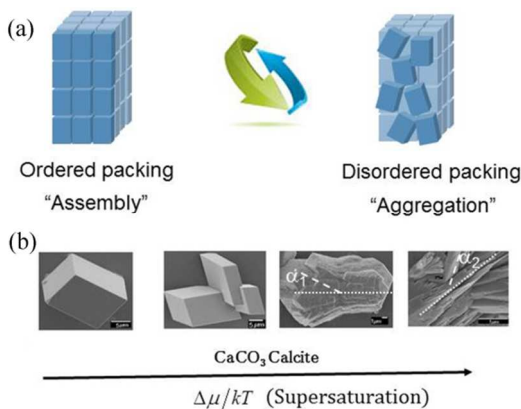


Fig. 19 (a) Schematic illustration of assembly and aggregation under the influence of ordered structure. (b) Supersaturation Driven Interfacial Structure Mismatch Nucleation: the structural match between the daughter crystals and the parent crystal will become poor as supersaturation increases. Reproduced with permission from Ref. ²⁶. Copyright 2012 Springer.

Fig. 19b reveals the transition from the neat growth to the ordered stacking (assembly) growth, finally to the aggregated growth of calcite crystals. As indicated, such the sequential pattern transformation occurs as supersaturation increases. This therefore refers to supersaturation driven interfacial structure mismatch nucleation mediated branching.

As mentioned in Section 2.2, the growth of tip faces of needle crystals is either in the rough mode or in the faceted growth mode. If the substrate is a growing crystal itself, the optimal structural match means that the new layer on the surface of the growing crystal matches exactly the crystallographic orientation of the parent crystal. This corresponds to the growth of crystalline fibers in common sense. However, once some mismatch occurs between the parent crystals and the nucleating layers of crystals, the new crystal growing layers will deviate from the optimal structural match position.^{49a} It follows then that daughter crystallites often occur via heterogenous nucleation (templating) on the top of the parent crystal surfaces.

A large degree of mismatch/misalignment between the daughter and parent crystallites will give rise to a higher interfacial energy than the matched nucleation. According to Eqs. (6) and (7), the mismatched templating will correspond to a much higher nucleation barrier at low supersaturations, than the matched templating (Fig. 19). This prevents the mismatch nucleation from happening at low supersaturations. This explains why the formation of the ordered HAP assembly observed in Figs. 16b and 19b at low supersaturations. As the supersaturation increases, the nucleation barrier for mismatch epitaxial nucleation drops rapidly (Fig. 20).

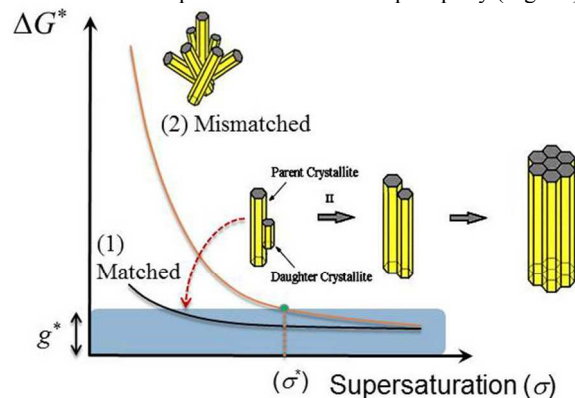


Fig. 20 The nucleation barrier of disordered/mismatch packing with supersaturation, compared with ordered/matched packing.

As supersaturation increases, the mismatch/misaligned structural packing will be obtained. The disordered assembly of crystallites (Fig. 20) is obtained. The orientation of crystallites will be less ordered and open in this region. The crystal networks acquired will be open and porous.

We notice that the transformation of crystallites stacking or assembly manner often gives right to the variation of network topology, which often results in the variation of macroscopic performance of mesoscopic materials. In section 5, more details will be given to addressing this subject.

4.3 Mechanism of fibrous/crystal network formation and topological variation by branching

As indicated by table 1, the different topologies of crystal networks often lead to macroscopic performance of materials. In other words, the tuning of the properties of mesoscopic materials can be achieved by modifying the key factors of crystal networks, in particular, the

variation of the topology. In this regard, the control of the crystal network formation and/or the promotion of the topological verification are crucial.

One of the most important routes to create the networks of fibers or crystallites in mesoscopic materials is to promote fiber branching/molecular merging, as described by section 4.2.

During the growth of crystals, there is a tendency of randomness of growing new layers with respect to the surface structure of the parent crystals. At low supersaturations, such randomness is suppressed due to a very high nucleation barrier (Fig. 19). However, at high supersaturations, the mismatch nucleation barrier is greatly suppressed (Eqs.(6) and (7)). This leads to the creation of new crystallites in deviated orientations on the surface of the parent crystals. Similar to normal nucleation, the mismatched crystallites should first nucleate on the growing crystal surface. If the energy needed to create a mismatch domain per area on the parent crystals is defined as the specific mismatch free energy γ_{mis} , the barrier of mismatch nucleation is determined by surface supersaturation and γ_{mis} (Eqs. (6) and (7)). The crystallographic mismatch nucleation is a special case of heterogeneous nucleation, where $\gamma_{\text{mis}} = \gamma_{\text{sc}}$. If the mismatch growth does not deviate much from the crystallographic orientation of the parent crystals, we can in principle have $\gamma_{\text{cf}} \sim \gamma_{\text{sf}}$. It follows then that

$$m = 1 - \gamma_{\text{mis}} / \gamma_{\text{cf}} \quad (17)$$

As indicated by Eqs. (9) and (10), ΔG_{mis}^* ($\Delta G_{\text{hetero}}^*$) decreases as the supersaturation increases. Notice that the only difference between normal heterogeneous nucleation and the crystallographic mismatch nucleation is that in the crystallographic mismatch nucleation, the substrate is the growing crystal surface, whereas in normal heterogeneous nucleation, substrates are foreign bodies. Similar to normal heterogeneous nucleation, crystallographic mismatch nucleation and growth is controlled by the following factors:

(1) *Thermodynamic driving force (supersaturation).*

At low supersaturations, the crystallographic mismatch nucleation is difficult to occur due to the high ΔG_{mis}^* (Eqs.7 and 8). As supersaturation increases, ΔG_{mis}^* will drop rapidly (Fig. 20). There are a number of ways to acquire high supersaturations: (i) the low solubility of solutes: based on Eq.(3), if the solubility of a solute in a solvent system is low, one can achieve a high supersaturation easily. This is why an effective small molecular gelling agent normally has a very low solubility; (ii) Normally, the precipitation of gelling molecules from the liquid phase will cause the drop of the supersaturation quickly. To avoid the quick reduction of thermodynamic driving force, quenching a solution from a high temperature to a low temperature can be an effective way to build up high supersaturations.

(2) *Impurities.* Adsorbed impurities may disturb the interfacial structural match between nucleating layers and the parent crystal surfaces. This lowers m and promotes crystallographic mismatch nucleation.

(3) *Slow surface integration.* Crystallographic mismatch nucleation is governed by surface supersaturation. The orientations with slow surface integration kinetics will therefore lead to higher surface supersaturations that are closer to the bulk supersaturation. It follows that at low supersaturations, the crystal faces with slow surface integration kinetics can take advantage of the highest possible supersaturation—the bulk supersaturation of the system, and will induce the crystallographic mismatch nucleation more easily.

(4) *Low specific mismatch free energy.* According to Eqs. (6, 7, 8), a low specific mismatch free energy γ_{mis} leads to a low ΔG_{mis}^* . This implies that the crystallographic mismatch nucleation can occur

much more easily on crystal surfaces with low γ_{mis} . Normally, crystal surfaces with low γ_{mis} often coincide with those with slow surface integration kinetics. Therefore, criteria 3 and 4 may be very likely applied to the same crystallographic orientation for a given crystalline material.

According to the above analyses, the formation of crystal networks occurs via the self-epitaxial nucleation and the topological variation and/or the ordered-disordered transformation are to a large extent controlled by the crystallographic mismatch nucleation.^{13, 18c, 32, 35, 49a} On the basis of criteria 1 and 3, we can expect that at high supersaturations, the crystallographic mismatch nucleation may occur in faster growth crystallographic orientations. Whereas at low supersaturations, the crystallographic mismatch nucleation takes place more easily in slow growth crystallographic orientations. Another reason for the occurrence of crystallographic mismatch nucleation in faster growth crystallographic orientations at high supersaturations is that the faster growth crystallographic orientations can penetrate into the bulk easily, and “feel” much higher supersaturations in the bulk. This will trigger the crystallographic mismatch nucleation at the tips.

In the following sections, we will present the fiber network construction through branching at different orientations of fibers, that is, at the growing tips and side surface of fibers. Three typical branching mechanisms of branching are (a) Tip splitting/branching; (b) type I side branching, and (c) type II side branching/merging. The various branching processes are illustrated by Table 1. The tip splitting/branching and the side branching belong to the one-step process and mixed mode of assembly. More details are given in the following section.

4.3.1. Fiber tip branching

As discussed, at high supersaturations, the crystallographic mismatch nucleation and growth will take place at the tips, leading to fiber tip branching (see Fig. 21a and 24b). The formation process of a fiber network through tip branching has been shown in Figs. 20a and 23b. This type of fiber network consists of radius arms initiating from a primary nucleation center through 3D nucleation. The radius arms are often found to be branched with the Cayley tree structure.⁷⁰ Taking into account this fact and the structural characteristics of a Cayley tree of fibrous networks, the process for the network formation can be regarded as: *primary nucleation—growth—branching—growth—branching*. Obviously, one of the key steps in building up the Cayley tree is the branching at the tips of growing nanofibers. Unlike dendritic branching, the daughter branches of the fibers cannot be correlated strictly to the crystallographic orientation of their parent fibers. Therefore, the branching is referred to as *crystallographic mismatch* (or *noncrystallographic*) branching. The kinetics of the branching kinetics can be given as follows.

The kinetics of fiber growth is generally controlled by a 2D nucleation (birth-and-spread) growth mechanism. This implies that the growth of crystal faces in the normal orientation (the fibril axis orientation in our case) takes place by growing crystal layers on top of the existing surface, and the occurrence of a new layer on the existing layer is controlled by 2D nucleation. The growth rate, R_g of fibers in the fibril axis direction can be calculated from Eqs. (12, 13).

Designating the induction time for the nucleation of new fibers on the host fibers as t_g ($t_g \sim 1/J$), the average branching distance can be expressed as

$$\langle \xi \rangle \sim R \cdot t_g \sim R/J \quad (18)$$

$$\langle \xi \rangle \approx C_2 \beta_{st} \frac{(\Delta\mu/kT)^{5/6}}{f^n f^{1/2}} \exp \left\{ \frac{16 \pi f}{3(\Delta\mu/kT)^2} \left(\frac{\gamma_{sf} \Omega^{2/3}}{kT} \right)^3 \right\} \quad (19)$$

where $C_2 = (C_1/4\pi\alpha (R^S)^2 B)$. The branching kinetics described by Eq. (19) has been verified for many gel systems. In a recent work, the crystallographic mismatch induced fiber branching of a small molecule gelator 12-hydroxyl stearic acid (HSA) was examined on a molecular scale using synchrotron Fourier transform infrared (FTIR) spectroscopy.⁷¹ It was observed that the branching distance of the HSA fibers were influenced by crystallographic mismatches resulting from the incorporation of HSA monomers into the crystal lattice in an imperfect manner.

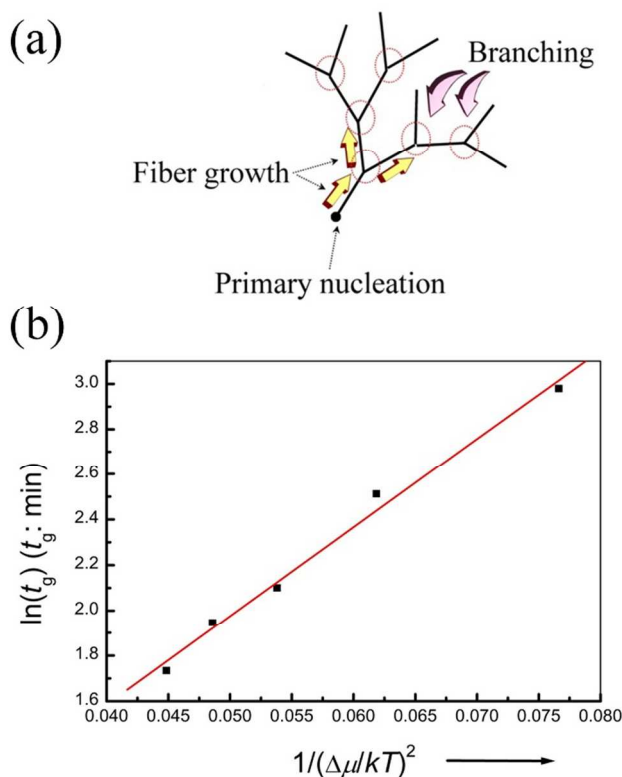


Fig. 21 (a) Illustration of crystal network formation by fiber tip splitting/branching. The branching occurs via *crystallographic mismatch* branching. Apart from crystalline fibers which occur via three dimensional primary nucleation, the growth of crystalline fibers is generally controlled by a 2D nucleation (birth-and-spread) growth mechanism. Due to the occurrence of thermodynamic, chemical, sound, and other stimuli, the mistakes or defects would occur on the growing layers at the tip of fibers. This leads to the *crystallographic mismatch* branching, and the modification of topology of fibres. The continuous branching in a given sequence will give rise to the formation of fiber networks as summarized in the second row in table 1. (b) The correlation between $\ln[\langle \xi \rangle (\Delta\mu/kT)^{-1}]$ and $1/(\Delta\mu/kT)^2$ for a gel formed with a polymer additive at 20°C. The linear relationship confirms the governing role of the crystallographic mismatch branching mechanism in the formation of organized interconnecting fiber networks. Reprinted with permission from Ref. ³⁵. Copyright 2002, American Chemical Society.

4.3.2 Fiber side branching

At relatively low supersaturations, owing to the large ΔG_{mis}^* , the crystallographic mismatch nucleation and growth will only occur at

the side faces of needle crystals as these faces are the slowest growing directions and thus have the largest effective surface supersaturation. This leads to side branching (type I). At low supersaturations, single fibers form first without any branching, as the free-energy barrier ΔG_{mis}^* is very high. As supersaturation increases (ΔG_{mis}^* is reduced), the branching of fibers initiates from the side faces. With further increase supersaturation, ΔG_{mis}^* at the growing tip of fibers becomes very low and tip branching is favoured. The 3d row of Table 1 describes the side branching of fibers based on the microscopic observation.

4.3.3 Fiber/polymeric side merging

Fiber side branching can also occur by side merging of polymer chains (Table 1). This type of branching is normally observed in polymer gels. On the basis of electron microscopic images and MD simulation, the proposed mechanism is as follows: the fiber branching takes place in four steps.²⁹ Firstly, the polymer chain is stiffened due to intramolecular hydrogen bonds after quenching (step 1). At this stage, the polymer chain with limited flexibility becomes rigid, which facilitates the formation of nuclei in terms of the primary self-epitaxial nucleation (step 2); the primary nuclei serve as the substrate for other oncoming stiffened chains following the same mechanism (step 3). This process thickens the nanofiber. Meanwhile, the epitaxial growth of the existing nuclei lengthens the fiber (step 4).^{29, 72}

5. Engineering of supramolecular soft materials by mesoscopic crystal network (re)construction

While the correlation between the structure and the performance of mesoscopic materials with network structures was covered in Section 2 and 3, the formation kinetics of mesoscopic crystal networks has been discussed in Section 3 and 4. Recently, it was found that crystal networks do exist in many soft materials, i.e. supramolecular gels, spider and silkworm silks and the derivatives.^[4,6,15,18-22,35,81] Nevertheless, most people only care about the gelation properties from the aspect of chemistry, without paying much attention to the effect of crystal networks. As the crystal networks turn out to be one of the key mesoscopic structural components in soft materials, insufficient understandings on the formation of crystal networks and the correlation between the structure of crystal networks and the performance of materials cause many “doubts” in the society of materials research.^{18f} On the other hand, a descent understanding of the structure and formation mechanisms of crystal networks will allow identifying more effective strategies in designing and “formulating” soft materials. For instance, the factors which affect the crystal network formation kinetics, outlined in Sec 4.3, can be further developed to the strategies for the engineering and fabrication of supramolecular materials. We will in this section highlight how the principles can be applied to the development of such strategies.

For a soft material with the domain structure, the rheological properties of the material depend on both the structural characteristics of the multi-level networks and the interactions among them. As mentioned before, the most important parameters of fiber networks are the topology, the correlation length ξ (or average branching distance) of the networks, the ordering or symmetry of crystallites and the interaction among structural units. Here, the fabrication of molecular or supramolecular gels is of two fold implications: (a) branching/networking (the change of topology) or (b) tuning the branching density of materials at mesoscopic scale (the altering of the correlation length ξ) (Fig. 22). As the change in

the branching state can lead to the variation of topology. Generally speaking, we can refer it to *topological variation*.

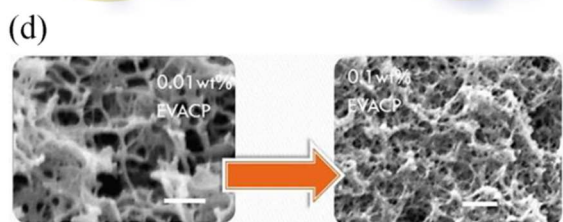
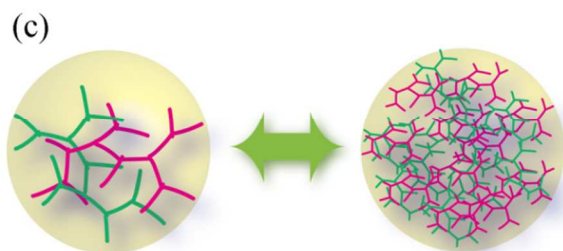
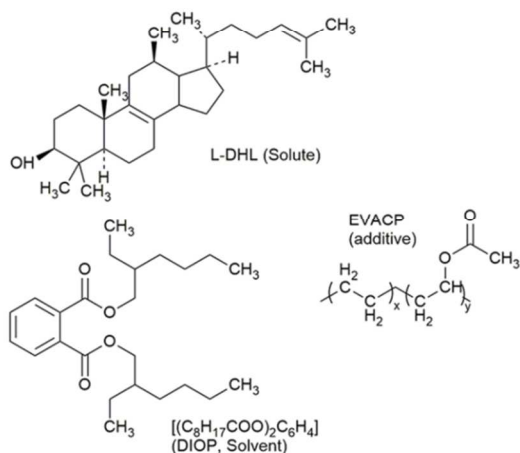
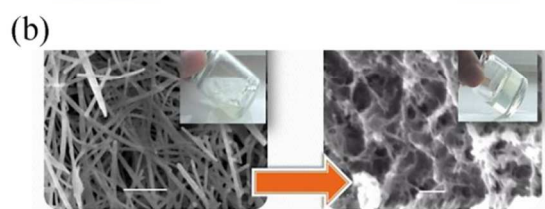
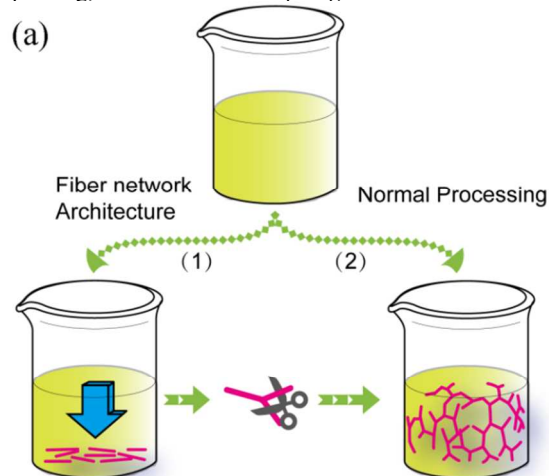


Fig. 22 Illustrations of network construction by the topology variation of crystallites. (a) creating branching/networking or (c) tuning the branching density. (b) SEM image of a gel of unbranched L-DHL fibers formed in DIOP in the absence of additive (left image) and the corresponding fiber network of L-DHL formed in the presence of EVACP (right image). (d) SEM images of enhanced tip branching by adding more additive EVACP. Reprinted with permission from Ref. ³⁵. Copyright 2002 American Chemical Society.

Notice that as long as the crystallites are involved in the network formation, the nucleation and growth of the crystallites will govern the formation of the mesoscopic structure of materials. In the following discussion, we will first focus on the crystal networks/domain network fabrication.

5.1 Engineering in the mesoscopic structure of fiber networks by branching stimulation (topological variation)

As mentioned before, the change in branching state leads to the variation of crystal network topology. The strategy of crystal networks fabrication (or topological variation) can be implemented by promoting mismatch nucleation (Fig.23(B)). In Section 4.2, the basic approaches of engineering are those based on the criteria outlined by *mismatch nucleation mediated branching stimulating*, i.e. changing thermodynamic driving force or adding tailor-made additives, etc. The main approaches and the principles are illustrated by Fig. 23.

5.1.1. Engineering of crystal networks by thermodynamic driving force

As indicated in Section 4, supersaturation, the thermal dynamic driving force of crystallization, is one of the main parameters in controlling the fiber branching. Supersaturation does not only affect the nucleation rate, but also affect fiber branching by decreasing (at higher supersaturation) or increasing the structural match (at lower supersaturation) between the nucleating phase and the substrate (fiber). Different supersaturation can be obtained by changing the temperature for gel formation at a fixed concentration of gelator, or by keeping the temperature while changing the gelator concentration.

As shown by Fig. 23(A), ΔG_{mis}^* is a parameter to describe the condition under which the branching will take place. In other words, this is a kinetic barrier in making a topological change. As supersaturation rapidly increases, ΔG_{mis}^* will drop as well (Fig. 23(A)). Mismatch nucleation leads to the branching and formation of crystal networks.

The effect of supersaturation on fiber branching has been quantified for some molecular gels. There have been a large number of cases reported concerning the tuning of branching and the network structure of crystal networks in the various supramolecular gels.^{18c, 24, 28-29, 31, 35, 69b, 72b, 73} For example, for a gel formed by *N*-lauroyl-*L*-glutamic acid di-*n*-butylamide (GP-1) in isostearyl alcohol (ISA), the effect of thermodynamic driving force (supersaturation) on branching of fiber crystal networks in supramolecular gels is demonstrated by Fig. 23(C)(A and B).⁴² A higher thermodynamic driving force enhances the mismatch nucleation rate and fiber branching, leading to gels of a smaller ξ (Eq.(19), Fig. 23(D)).^{35, 73b} This can be quantified by Eq.(19). the G' decreases exponentially with the branching distance/correlation length $\xi(G' = 1.07 \times 10^6 \xi^{-0.49})$ (c.f. Fig.9a).

Apart from supersaturation, cooling rate is another important factor describing thermodynamic driving force that determines the

network structure. A higher cooling rate (to accumulate supersaturation in a short time) led to the formation of thinner and densely branched fibers (Fig. 23(C)-A, B). It was demonstrated that the network formation in molecular gels such as agarose gels was also controlled by nucleation^{13, 18c, 24, 31-32, 35, 41a, 69b, 74}

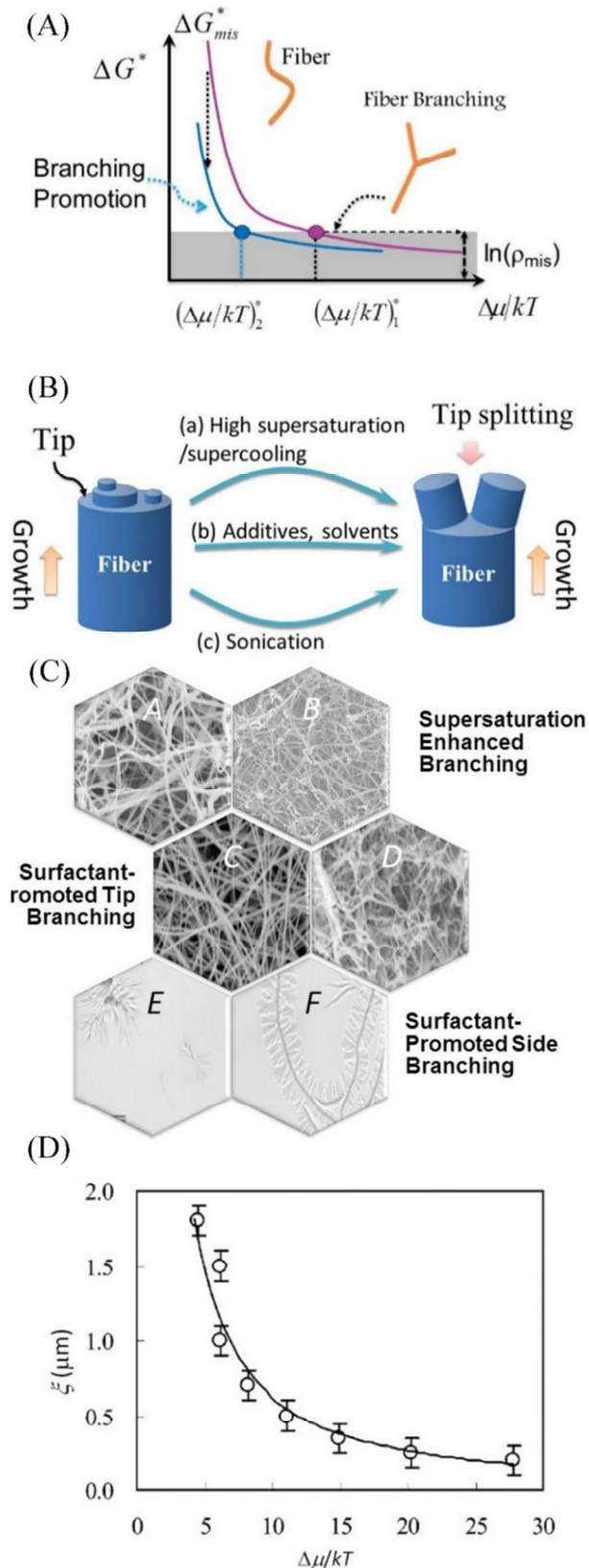


Fig. 23 (A) Illustration of the effect of supersaturation and other stimuli on the energy barrier for mismatch nucleation. (B) Illustration of fiber growth and branching through the birth-and-spread mode, branching can be enhanced with stimuli. (C) SEM images: enhanced tip branching by: raising thermodynamic driving force (the driving force of B is higher than that of A); surfactant-promoted fiber tip branching C and side branching (HSA fibers formed in lanosterol without surfactant and D with Tween 80); enhanced side branching by surfactant: GP-1 fibers formed in PG, E without surfactant, F with increasing concentration of span 20. Reprinted with permission from Ref. 69b and Ref. 24. Copyright 2009, Wiley-VCH, and copyright 2009 Wiley-VCH. (D) The effect of supersaturation on the correlation length of fiber networks. A small molecule organic gelator, N-lauroyl-L-glutamic acid di-n-butylamide, grown from an isostearyl alcohol solution. The fitting of the data is based Eq. (19). Reprinted with permission from Ref. [6c], Copyright 2005, ACS.

5.1.2 Engineering of crystal networks by topological modifiers

The agents leading to the change in branching state or topological variation is defined as *topological modifiers*. Here the so-called topological modifiers refer to the impurities or tailor-made additives outlined in Sec. 4.3. To stimulating breaching by crystallographic mismatch nucleation, a suitable *topological modifier* should adsorb strongly on the surface of growing fibers to interrupt the structural match between the nucleating phase and the surface of growing crystal fibers. Therefore, the selection of additive is not arbitrary. On the basis of the results obtained from theoretical calculations and experimental observations,⁷⁵ we provide some guidelines as follows:

(1) Large molecule with a relatively rigid basic structure. The rigidity of additive molecules can result from a variety of molecular features, such as the intra molecular bonding (i.e. hydrogen bonds, double or triple covalent bonds) and the presence of bulky functional groups in the backbone of the molecules. Based on both energetic and entropic consideration, for different molecules of similar types, larger molecules with somewhat rigid structures are easily adsorbed at interfaces.^{75b, 75c}

(2) Stronger interaction between additives and the substrate will lead to a stronger adsorption at the surface.^{75a-f} Since the surface of crystals is highly ordered and stiff, to obtain the maximal interactions by matching the structure of the substrate, it is desirable to have short and relatively flexible functional groups attached to the backbone of additives molecules so that they can adjust their positions to obtain optimal interactions with the solid molecules at the surface of crystals.

(3) The adsorbed additives should interrupt the growth of crystal layers along the substrate.^{75a-f} The repulsions can originate from steric, electrostatic, polar/non-polar, or hydrophilic/hydrophobic forces, and can be achieved by attaching some functional groups to the backbone of the molecules of additives.

Large molecules such as polymers with molecular structure that satisfy the above criteria have proven to be effective. Beside polymers, surfactants are a class of chemicals that have interfacial adsorbing property. Due to its amphiphilicity, a surfactant molecule can adsorb at the interface of two phases with different polarity to minimize the interfacial tension and free energy. Therefore, surfactants can also be suitable additives.

(a) Polymeric additives

Tailor-made additives, in particular, polymeric additives, have been chosen as branching promoters in directing the formation of three dimensional fiber networks. As shown by Fig. 22a, a tiny amount of an ethylene/vinyl acetate copolymer (EVACP) additive

was found to be able to construct 3D crystal networks of L-DHL (lanosta-8,24-dien- β -ol: 24,25-dihydrolanosterol = 56 : 44) in the solvent di-(2-ethyl-hexyl) phthalate (DIOP) (Fig. 22b) by branching promotion.³⁵ Without this additive, L-DHL crystallized into unbranched short fibers (Fig. 22b, left image), which are a paste-like material. The branching promotion by this polymer is due to its strong adsorption on the tip surface of L-DHL fibers, which leads to mismatch nucleation.

(b) Surfactants

Both enhanced tip and side branching of fibers were achieved using different surfactants. For example, the presence of a tiny amount of Tween 80 enhanced the tip branching of GP-1 in ISA. Without the surfactant, elongated fibers with a low degree of branching (Fig. 23(C)C) were formed at low supersaturation of GP-1. The branching distance of the GP-1 fibers was decreased from 2.5 μ m to 400 nm (Fig. 23C (D)). Similar effects of this surfactant on the branching of lanosterol fibers formed in benzyl benzoate were also observed. The presence of Span 20 enhanced the side branching of GP-1 fibers formed in propylene glycol (PG), which converts spherulitic fiber structures into comb-like and brush-like fibers (Fig. 23C(E-F)).

5.1.3 Engineering of crystal networks by ultrasound/external fields

Among a variety of external physical stimuli, light⁷⁶ and electric fields⁷⁷ have been successfully used to switch molecular aggregations involved in the formation of gel, micelles, vesicles, and membranes. However, developing a method that can control the hierarchical structure of molecules/crystal networks remains as a challenge. Ultrasound has been known to be a powerful stimulus in the field of sonochemistry because of its diverse physical and chemical effects, such as cavitation, agitation, acoustic streaming, diffusion, and mechanical rupture for many decades.⁷⁸ However, it is only very recently that it was used to manipulate the formation of crystal fiber networks.⁷⁹ On one hand, ultrasound was observed to induce the mechanical disruption of molecular aggregates by cleaving the noncovalent bonding, leading to the suppression of a gelation process and the rupture of the gel network.⁸⁰

The architecture of self-organized three-dimensionally interconnected nanocrystal fibrillar networks has been achieved by ultrasound.⁸¹ The ultrasound stimulated structural transformation is correlated to the striking ultrasonic effects on turning non-gelled solutions or weak gels into strong gels instantly, with the enhancement of the storage modulus up to 3 magnitudes, and of 4 times in the gelling capability.

There are two counter effects of ultrasound in supramolecular gels fabrication. Constructive use of ultrasound was demonstrated in 2005 with two reports of ultrasound-induced gelation ("sonogelation").^{79d, 82} On the other hand, many molecular gels (and other materials) are damaged or destroyed by the excessive and lengthy application of ultrasound⁸³, due to the fact that the structure of fibrillar crystal networks was broken down by sonication. Although the negative effect of ultrasound in the molecular aggregation has been studied extensively and is well-understood, the principle of the positive effect of ultrasound on altering the topology of crystal networks remain to be examined.

Fig. 24(B) reveals a gelation case of 2 wt % GP-1/PG sample. A weak gel/or viscous flowing fluid was obtained in a normal processing without ultrasound stimulus.⁸¹ Such a liquid is composed by the closely packed spherulites (Fig. 24(B)a). Under the same composition and thermal treatment, the sample became a self-supporting solid gel in applying a short period of ultrasound during gelation (Fig. 24(B)b). As revealed by Fig. 24(B), ultrasound induces

the transformation from the spherulites to 3D interconnected fiber networks, leading to the significant impact on the rheological properties. As shown in Fig. 24(B)c, the storage modulus G' of the ultrasound-modified gel for the 2 wt % GP-1/PG is one magnitude stronger than the untreated gel.⁸¹

The above example demonstrates that ultrasound is capable of switching from a non-gelled to a gelling state, or a weak gel into a strong gel.

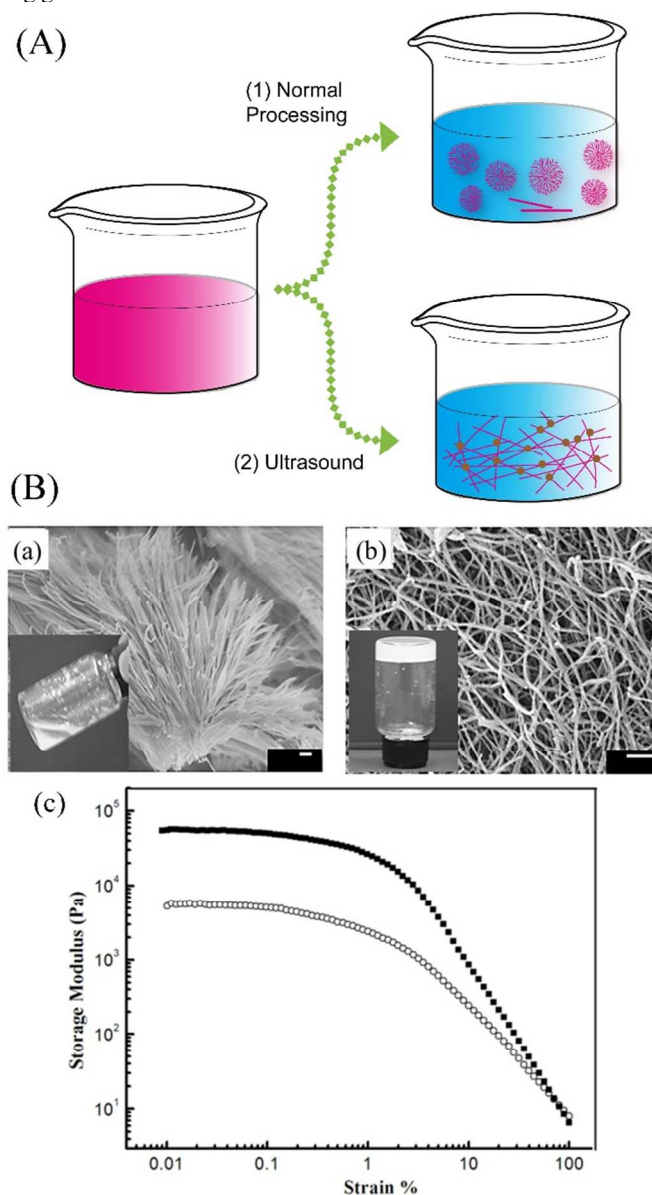


Fig. 24 (A) Illustration of micro/nanostructure engineering of soft functional materials: the control of kinetic pathway by ultrasound (route 2) with respect to normal fiber network formation (route 1). (B) SEM micrographs of GP-1/PG gel samples. (a) Spherulitic domains formed without ultrasound; (b) 3D interconnected fiber network formed with 1 minute of sonication treatment. Scale bar: 500nm. (c) The storage modulus G' of the GP-1/PG gels formed without ultrasound (○) and with ultrasound (■), respectively. Reprinted with permission from Ref.⁸¹. Copyright 2009, American Chemical Society.

As long as crystallization is concerned, the control of nucleation and growth is always the center of interests. Regarding the crystal network formation, high supersaturation often leads to the spherulitic growth and a multi domain networks. The high supersaturation growth is normally caused by the difficulty in primary nucleation, which often occurs in organic, and various macromolecules, and the normal crystallization with the effect of additives. Nevertheless, nucleation, both primary nucleation and secondary nucleation, can be promoted by ultrasound, so that the aforementioned crystallization and crystal network formation can be initiated at the low supersaturation regime. Low supersaturations give rise to the side branching and less dense branching during crystal networks formation. This consequently causes the variation of topology in the newly formed crystal networks. (Fig. 24).

Apart from ultrasound stimulus, electric and magnetic are in principle capable of stimulating the similar transformation.⁸⁴ These techniques enable people to produce self-supporting soft functional materials possessing significantly modified macroscopic properties from the materials previously thus far considered to be “useless”, without the use of chemical stimuli.

5.2 Engineering of soft materials by tuning domain network structure

As indicated by Fig.3, mesoscopic soft materials often consist of hierarchical networks. To a large extent, the different levels of structures can influence the macroscopic performance of materials synergistically. In the case of supramolecular gels (c.f. Fig.3), the weak inter domain interactions (in the domain network) to a large extent determine the macroscopic performance of soft materials. In this regard, the density of the crystal network domains determines the mechanical properties of the materials. In a domain network, each single network domain initiates from a primary nucleation centre. Therefore, in a given volume, the number and size of single networks is directly correlated to the primary nucleation. In other words, the control of the domain network structure in a system is to control the primary nucleation in the system. A lower primary nucleation rate leads to the formation of a smaller number of nuclei, which leads to larger single networks in the end. This will improve the mechanical properties of the materials since it reduces the mechanically weak boundary areas between the single networks. Therefore, in terms of obtaining materials with better mechanical properties, reducing the primary nucleation rate is an effective approach.

The primary nucleation rate can be controlled by a variety of means. These include tuning the thermodynamic driving force, or employing suitable additives to activate/inactive some nucleation centers (Fig. 25). Adding nucleation seeds or applying external fields can also be very effective (Figs.26-28) in modifying the domain network structure. Finally, volume confinement is also an effective approach.^{45a, 45b} The different approaches and typical examples are demonstrated as follows.

5.2.1 Thermodynamic driving force stimulus control

The influence of thermodynamic driving force is demonstrated by Fig. 25a &b. Lowering thermodynamic driving force reduces the primary nucleation rate, which leads to the formation of larger single networks in the domain network. Correspondingly, this significantly enhance the G' of materials. For example, for the gels formed by GP-1 (3 wt %) in propylene glycol (PG), the G' are 4.7×10^4 and 1.3×10^5 N/m² for the gels formed at 35 and 50 °C (Fig.25a&b),

respectively, which is almost three times increase due to the increase in sizes of single networks (Fig. 25b) Although reducing thermodynamic driving force can enhance the G' , it also reduces the fiber mass, which has a negative effect on G' . A gel will fail to form when the driving force is below a threshold. Therefore, an optimal driving force exists for a given system.^{6a}

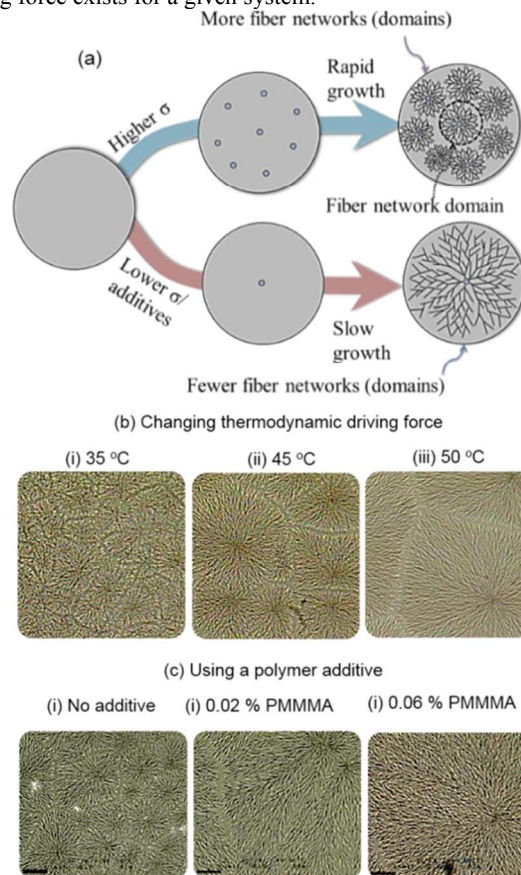


Fig. 25 (a) Illustration of controlling the size and number density of single networks in a multi-domain network. Engineering multi-domain networks through controlling primary nucleation by (b) reducing the thermodynamic driving force or (c) using a polymer additive PMMMA. The concentration of GP-1 was fixed for both (b) and (c). For (c), the temperature for gelation was fixed at 40 °C. Gels were formed by GP-1 in PG. (a) and (b) are reprinted with permission from Ref. ^{6a}. Copyright 2013 Royal Society of Chemistry. Images in (c) are reprinted with permission from Ref. ⁸⁵. Copyright 2009, American Chemical Society.

5.2.2 Chemical stimulus

Additives that inhibit the primary nucleation are also effective to promote the formation of stronger materials. For example, it was observed that a co-polymer additive poly(methylmethacrylate co-methacrylic acid) (PMMMA) could effectively inhibit the primary nucleation of GP-1 in PG. In the case of Fig. 25c, the primary nucleation rate was reduced by the addition to PMMMA the gels. As the primary nucleation is reduced, the G' of the gel could be improved more than five times. The advantages of the additive approach is that it does not to form the gels at high temperatures (low driving force), which is important if temperature-sensitive components are encapsulated in the gels.

5.2.3 Effect of foreign particulates or seeding

Regarding the control of primary nucleation, one cannot avoid the impact of foreign particulates or seeding. This is to introduce foreign particulates or seeds to promote heterogeneous nucleation, so as to control the domain number and network structure. Herein, we discuss the impact of foreign particulates or seeds on the rheological properties of regenerated silkworm silk fibroin (RSF) hydrogels and the hierarchical networks (Fig. 31).⁸⁶ Similar to other hydrogels and/or molecular gels, regenerated silk fibroin (RSF) hydrogels are of the hierarchical network structure, belonging to the case of weak (nanofibril) domain-(nanofibril) domain interactions as illustrated by Fig. 3A(b). In this case, a gel RSF solution contains sufficiently silk nano β crystallites. Then, the nucleation density in a fresh silk fibroin solution can be acquired by mixing the fresh RSF solution with different volumes of the RSF gel solution of the same concentration (2%) at the ratios of 1:0 (1x), 1:1 (2x), 1:3 (4x) and 1:7 (8x). Consequently, the nucleation density from (1x), 1:1 (2x), 1:3 (4x) and 1:7 (8x), was reduced by up to eight fold, so was the domain density in the fresh RSF solution. Rheological data shows that both gelation time and storage modulus of samples with lower nucleation density are higher than samples with higher nucleation density (Fig.26). This is in line with our prediction as indicated by Fig.9b.

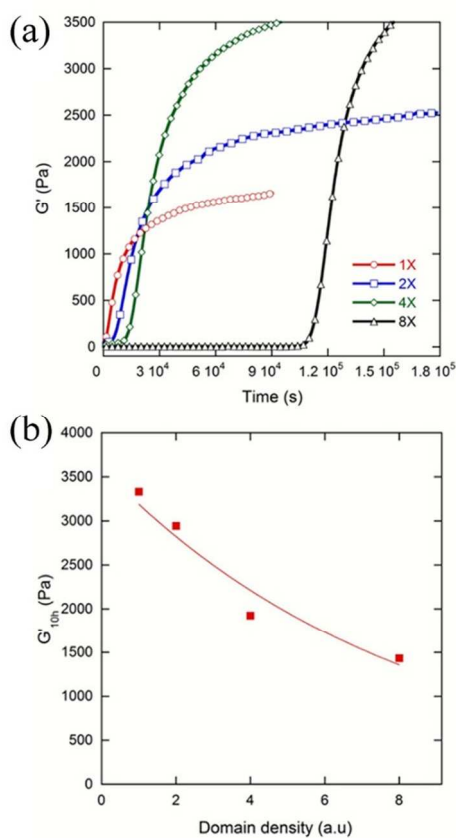


Fig. 26. (a) Rheological evolution and (b) dependence of the storage modulus G' on the seeding density of silk fibroin solution. Reprinted with permission from Ref. ⁸⁶. Copyright 2015, Wiley-VCH.

5.2.4. Effect of external field stimuli

Similar to the fabrication of crystal networks, external field stimuli, i.e. can also be applied to manipulate the domain networks of soft materials. In this regard, the impact of ultrasound on the structure is mainly achieved by the influence on the primary /secondary nucleation of crystal networks. As illustrated by Fig. 27, with the aid of ultrasound in combination with the thermal treatment, one can convert a non-gelling system to a strong gel with a three-dimensionally interconnecting fibrous network.⁸⁷

There are two effects in this concern. Firstly, ultrasound can promote nucleation in gelling solutions, so that crystal networks can occur at relatively low supersaturations (c.f. Sec 5.1.3).⁸¹ Secondly, ultrasound can break the existing crystal networks. The broken crystallites will then serve as seeds (Fig.26) in the gelling solutions. If one reduces thermodynamic drive force (by increasing temperature), the formation of crystal networks can proceed into the low supersaturation regime (the thermal treatment). The loosely branching of fiber networks are obtained, causing the interpenetration and interlocking of different crystal networks. Consequently, the domain networks will behave like a single crystal network (Fig.27).⁸⁸

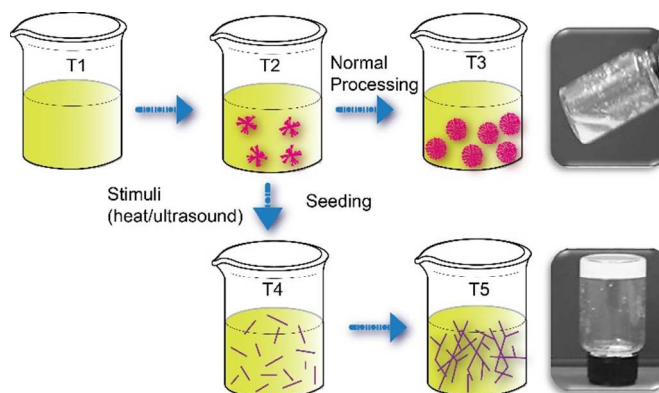


Fig. 27. Conversion of a multi-domain fiber network to a “single” crystal fibrous network through ultrasound-assisted fiber network formation. Schematic description of the formation of spherulites (opaque liquid) through the normal thermal processing and the formation of an interconnecting fiber network through ultrasonic stimulus. $T_1 > T_c > T_5 > T_4 = T_2 > T_3$, T_c is defined as the critical temperature, above which the gelator is totally dissolved. For ultrasound treatment, seeds are formed by mechanically breaking down the spherulites into fiber segments by ultrasound. Elevating temperature from T_4 to T_5 (low thermodynamic driving force) leads to loosely branching of fibre networks, causing the interpenetration and interlocking of different crystal networks. The domain networks will behave like a single crystal network (gelation). Photos are reprinted with permission from reference⁸⁸, copyright 2006, American Chemical Society.

If one only apply ultrasound stimuli to a gelling solution, primary nucleation will be promoted, which will then give rise to the increase of the domain number. Fig.28 reveals an example of silk fibroin hydrogel formation, where ultrasound was employed to promote the gel formation. Similar to the case revealed by Fig. 26, silk fibroin nanofibrils grown from the solution will be promoted by ultrasound, which results in a quick increase in the β crystallites in silk fibroin solutions. In this regard, the number of primary nuclei are proportional to the ultrasonication time and power. Therefore, a longer exposure time of ultrasonication will induce more nuclei of β crystallites, consequently a higher density of silk fibrous networks (domains) in the gels. According to Fig.9b, this will finally end up

with the reduction in the storage modulus G' of regenerated silk fibrin hydrogels. This is confirmed by Fig. 28b.

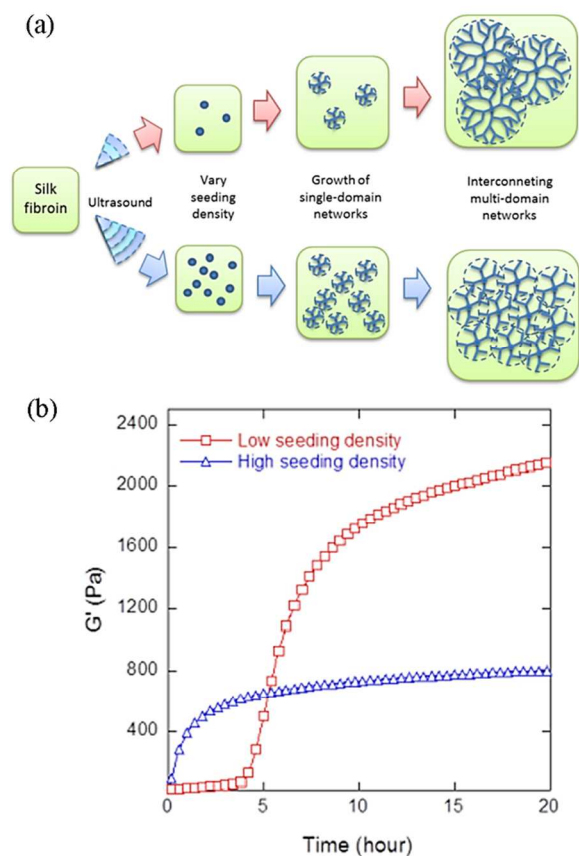


Fig. 28 Illustration of the strategy of controlling the mechanical property of silk fibroin hydrogels by controlling the hierarchical network structures, i.e. varying the density of nucleation centers. (a) Illustration of the ultrasound promotion of the primary nucleation and the formation of regenerated silkworm silk fibroin (RSF) networks and gels, which gives rise to a high density of primary nucleation and RSF networks/domains. (b) Ultrasound causes a high seeding (nucleation) density of RSF networks/domains (Δ) and a lower G' than the gels without ultrasounds in (\square). Reprinted with permission from Ref. ⁸⁶. Copyright 2015 Wiley-VCH.

6. Spider silk vs silkworm silk: from coupling of domain and molecular/crystallite networks to ultra-strong performance

Spider silk and cocoon silk fibers and derivatives, which are the materials with molecular β -crystal networks, are another class of soft materials with crystal networks.^{34d} The unusual combination of high strength and extensibility of spider silk fibers is a characteristic unavailable to date in synthetic materials yet. This biological template suggests new directions to emulate in the pursuit of new high-performance, multifunctional materials generated with a green chemistry and processing approach. The correlation between the performance and the structure of these materials can bio-inspire the fabrication of multifunctional material platforms that integrate with living systems for medical materials and a host of other applications.^{34d}

Silk derivatives include, i.e. silk hydrogels, films, sponges, belong to the soft materials with weak domain-domain interactions (Fig.3B(a)), whereas silk fibres are those with strong domain-domain interactions (Fig.3B(b)). The key macroscopic properties and the formation mechanism are the same as what have been highlighted in Sec 3-5. In terms of mesoscopic materials assembly/engineering,^{9a, 43-44, 86, 89} one can acquire functionalized silk fibroin based materials, i.e. silk photonic crystals and light emission materials-fluorescent silk fibres, films, sponges, etc. They are applicable in the area of biomedicine, bio imaging, due to their excellent biocompatibility and mechanical properties (Fig.29). They are also used for suturing, wound dressing, artificial ligaments, tendons, tissue scaffolds, etc. Silk fibroin regenerated from silk fibres can also be applied to fabricate different materials including micro/nano particles, gels, sponge and films for the biomedical applications. In this regard, the mesoscopic structure of the materials is of utmost importance concerning the bio-performance and functionality.^{9a} Apart from biomedical usefulness, these materials also have important applications in electronics, photonics and microfluids.^{34d, 90}



Fig. 29 Spider silk and cocoon silk fibres and regenerated silk derivatives, i.e. silk hydrogels, films, sponges, are soft materials with molecular β -crystal networks, In terms of mesoscopic materials assembly/engineering, one can acquire functionalized silk fibroin based materials, i.e. silk photonic crystals and light emission materials-fluorescent silk fibres, films, sponges, etc. They are applicable in the areas of biomedicine, bioimaging, tissue engineering etc.^{9a, 43-44, 86, 89} Reprinted with permission from Ref. ⁴³. Copyright 2015 Wiley-VCH.

On the other hand, we notice that spider silk and cocoon silk fibers belong to the soft materials with strong domain-domain interactions (Fig.3B(b)). We will discuss in this Section the correlation between the structural characteristics of the silk fibers and the macroscopic performance.

Silk fibers produced by spiders are one of the most intriguing natural material marvels owing to their exceptional mechanical properties, biocompatibility, and environment-friendly nature. As shown by Fig. 30, spider silk dragline fibers possess unique mechanical properties with a combination of superior strength and extensibility. *Nephila* dragline silk typically features an ultimate strength of 1.3 GPa, and an extensibility of 40%, giving rise to an unusual toughness of 160 kJ kg⁻¹, 5 times tougher than synthetic fibers, i.e. Kevlar.⁹¹

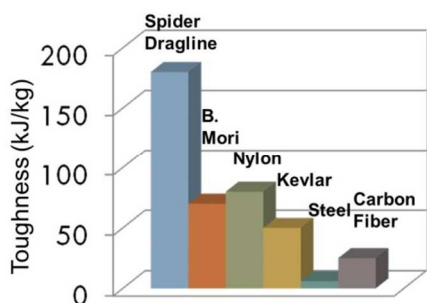
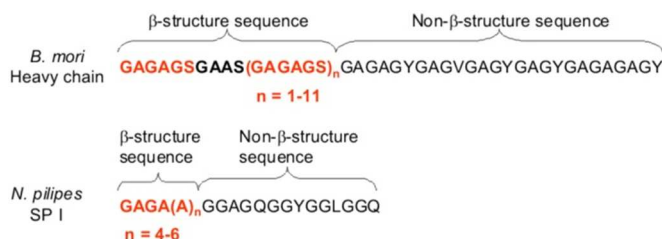


Fig. 30 The comparison of toughness between different fibers. The data were quoted from Ref.⁹².

Spider dragline silk fibers have a very high strength-to-density ratio, and are capable of absorbing great impact energy with low impact force at collision.⁹² In comparison, *Bombyx mori* (*B. mori*) silkworm silk fibers have weaker mechanical properties although the two types of silks share the similar nano and micro structures.⁹³ Notice that the major amino acids in the two types of silks are very similar. The primary structures of the two silks are as follows:



The secondary and the higher levels of structures of both spider and silkworm silks can be measured by various techs, i.e. X-ray scattering, fourier transform infrared spectroscopy (FTIR), raman spectroscopy, nuclear magnetic resonance (NMR) spectroscopy, etc. Based on the X-ray scattering and FTIR measurement,^{53, 86, 92, 94} the structural parameters of *Nephilapilipes* (*N. pilipes*) spider dragline silk and *B. mori* silkworm silk are summarized in Table 4.

It follows that although the total percentage of β -conformations (β -crystallites and intra β -sheets) for *N. pilipes* spider dragline silk and *B. mori* silkworm silk is very close to each other, the crystallinity (the percentage of β -crystallites) of *N. pilipes* spider dragline silk is only a half compared with that of *B. mori* silkworm silk. On the other hand, the volume of β -nano crystallites of *N. pilipes* spider dragline silk is only 1/4 of *B. mori* silkworm silk. This implies that the β -crystallite density of *N. pilipes* spider dragline silk is almost double compared with *B. mori* silkworm silk. Furthermore, the β -crystallite orientation of *N. pilipes* spider dragline silk fibers, described by orientation factor f , is better than *B. mori* silkworm silk fibers. (The orientation factor f describes the orientation of the β -crystallites along the fibre axis, $f = (3\cos^2\theta - 1)/2$, where θ is the angle between the c axis of the crystallites and the fiber axis. If $f=1$, β -crystallites are oriented completely parallel along the fiber axis. On the other hand, if $f = 0$, β -crystallites are oriented randomly.⁵³). We will see in Section 7.3, the above crystal network structural factors give rise to the much stronger *N. pilipes* spider dragline silk fibers than *B. mori* silkworm silk fibers.

Table 4. Comparison of structural parameters between silkworm silk and spider dragline silk fibers.

Sample name	Overall β -sheets (%)	Crystallinity (%)	Orientation function f	Crystallite size (nm)		
				a	b	c
Silkworm cocoon silk	42	40	0.84	2.3	4.1	10.3
Spider dragline silk	38	17	0.93	2.1	2.7	6.5

The latest researches indicate that silk fibers are of the hierarchical structure of crystal networks. The hierarchical structures of both *N. pilipes* spider dragline silk and *B. mori* silkworm silk fibers are given by Fig.29.

Here, a nano-fibril corresponds to a single silk protein molecular network, while a silk fiber, on the other hand, corresponds to a domain network. According to the latest results,^{86, 92, 94} a silk fiber consists of a bundle of nano-fibrils or “nano fibrous domains” (Fig. 31b). This corresponds to the case of the strong domain-domain interactions illustrated by Fig. 2B (b). Atomic force microscope (AFM) results reveal that each fiber is composed of numerous nano-fibrils with a diameter of around 30 nm for *B. mori* silkworm silks (Fig. 31b) and around 35 nm for *N. pilipes* spider dragline silk fibers. At the molecular-nano scale of the twisted nano-fibrils, nano β -crystallites, so-called the “nodes” in the networks of soft materials, are formed jointly by some adjacent silk protein molecules. In the following analysis, we will demonstrate that the strength of both silkworm silk and spider silk fibers are determined jointly by the molecular crystallite networks and the domain (nano fibrils) networks. In particular, the strong interactions between the adjacent domains (nano fibrils) will substantially strengthen silk fibers. We will in the following establish the correlation between the mechanical performance, in particular, the critical breaking point and the hierarchical structures of both spider and silkworm silks.

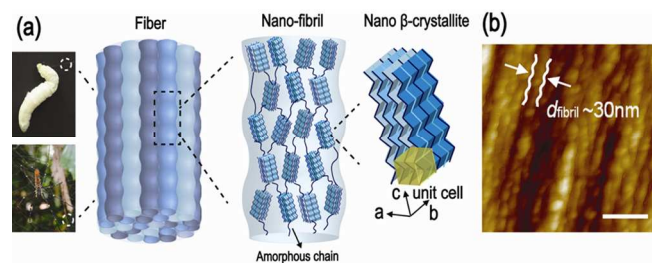


Fig. 31 The hierarchical structure of *Bombyx mori* silkworm and *Nephilapilipes* spider dragline silk fibers. (a) Both the silkworm silk and spider dragline fiber are composed of numerous interlocking nano-fibrils. Inside the nano-fibrils, the β -crystallites are connected by the amorphous chains to form a network. The β -crystallite is composed of stacked β -sheets with the peptide chains connected by the hydrogen bonds in each sheet. The yellow box indicates the unit cell of the β -crystallites and the coordinate indicates a (inter-sheet), b (inter-chain) and c directions. (b) AFM image of nano-fibrillar structure in *B. mori* silkworm silk with a sequence of associated segments (scale bar: 100nm). The β -structure sequence is GAGAGS GAAS (GAGAGS)_n, $n=1\sim 11$ for *B. mori* silkworm silks and GAGA(A)_n, $n=4\sim 6$ for *N. pilipes* spider silks (G: Glycine, A: Alanine, S: Serine).⁹⁵ Concerning the β nano crystallites, the lattice constants of the orthogonal unit cell of β -crystallites (Fig. 32a) are $a = 0.938$ nm, $b = 0.949$ nm, $c = 0.698$ nm for silkworm *B. mori* silks,⁹⁶ and $a = 1.03$ nm, $b = 0.944$ nm, $c = 0.695$ nm for spider *Nephila*

dragline silks.⁹⁷ As shown, the β -crystallites serve as the linkages connecting different silk protein molecular chains in nano fibrils. Reprinted with permission from Ref. ⁹⁴. Copyright 2014 Royal Society of Chemistry.

6.1 Mechanical performance of *N. pilipes* dragline and *B. mori* silk fibers

The typical mechanical performance of *N. pilipes* Dragline and *B. mori* silk fibers can be illustrated by Fig.31A.

In the linear region (elastic region in Fig. 30A), the amorphous chains are being stretched with the β -crystallites unaffected. After the yield point (point S in Fig. 32A), the nonlinear mechanical performance of silks is caused by the internal structural evolution. As the crystallites serve as the joints of the crystallite networks, the breakage of the fibers is initiated by the rupture of the β -crystallites.⁹² However, the mechanism of eventual breakage of the silk fibers is complicated due to the multi-levels of structures and the interactions between the structural units.

After the yield point, the spider dragline initially displays a characteristic J-shaped behaviour of strain-hardening (the slope of the stress-strain curves increases with strain) until point H, followed by a so-called strain-weakening behaviour (the slope of stress-strain curves decreases with strain) until the ultimate strength. It is found that other species of spider dragline silks follow the similar stress-strain profiles,⁹⁸ indicating that strain-hardening could be a general feature of spider draglines. On the other hand, the silkworm silk behaves only in the strain-weakening mode throughout its non-linear region of the stress-strain curve.

6.2 Spider silk fiber vs silkworm silk fibers: exceptional extensibility and strain hardening

Elastomers like rubber also exhibit a strain-hardening behaviour, which was attributed to strain-induced crystallization among the molecular chains.⁹⁹ Some semicrystalline synthetic polymers also have a very similar mechanism of strain hardening as that found for amorphous polymers.¹⁰⁰ Nevertheless, this mechanism is inapplicable to spider fibers because of the two major differences between silk and rubber. Firstly, rubbers are composed of completely random polymer chains, therefore the elasticity displayed in stretching rubbers is primarily due to the change in conformational entropy of molecular chains. In contrast, the amorphous chains in silk filaments are partially oriented with respect to the fibrous axis in its natural state, resulting in their mechanical behaviour remarkably different from that of rubbers.⁹³ Secondly, rubbers are amorphous polymers with simple structures,¹⁰¹ whereas silk exhibits much more complicated hierarchical structures. Evidently, the unique structural features of spider dragline silk result in the extremely high toughness and optimal extensibility that the spider uses to such great advantage in its web.

The structural origin of the stress-strain behaviour of spider dragline silk vs silkworm silk filaments has been investigated (Fig.32A).⁹² As indicated by table 4 and Fig. 31 and Fig. 32B, in the silk nano fibrils, the β -crystallites are jointly connected by several neighbouring silk protein molecules to form the molecular network. The non-crystalline β -sheets, so-called intra-molecular β -sheets, are merely normal β -sheets folded within individual silk protein molecules. For spider dragline silk, it was found that 38% of silk is in the β -conformation, of which 17% is in the β -crystallites (Table 4).⁹² This implies that the amount of intra-molecular β -sheets in *Nephila* spider dragline fibers is 21%. In contrast, 42% of fibrin molecules are in the β -conformation, among which 40% is in the crystalline. The amount of intra-molecular β -sheets in silkworm silk

fibers is 2%, almost negligible in comparison with *Nephila* spider dragline fibers. Fig. 32B demonstrates how the two structures contribute to their stress-strain profiles. Upon stretching after the yield point S in Fig. 32A, the intra-molecular β -sheets within the amorphous regions unfold first due to the fact that they are weaker. The unfolding gives rise to release the length of protein chains, while the β -crystallites remain unaffected. This leads to a high extension of draglines, without causing the breakage the inter-molecular linkage of molecular networks. It is noticed that at this stage, the modulus of silk fibres drops to nearly zero as the fiber extension is mainly caused by the breaking of weak intra-molecular hydrogen bonds. As the progressive unfolding and the alignment of protein chains continue, silk protein molecules and β -crystallites (nodes) of the molecular networks are stretched to bear the loading. Consequently, the silk filaments become stiffer due to the tightening of the networks (Fig. 32B). This is how strain hardening occurs in stretching spider dragline filaments. The further stretching beyond the inflection point H breaks the β -crystallites. This demolishes the crosslinks of the molecular networks in silk filaments and weakens the silk filaments (so-called strain-weakening).

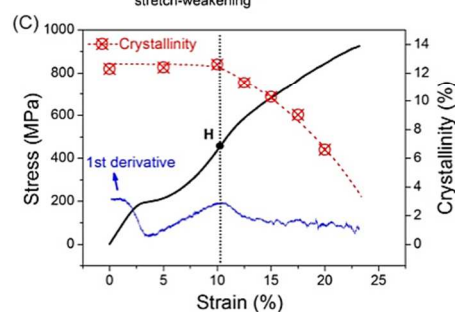
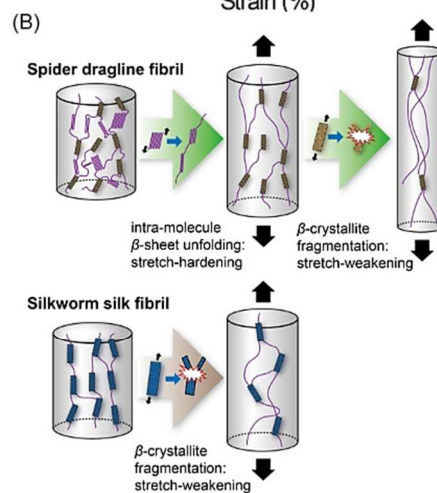
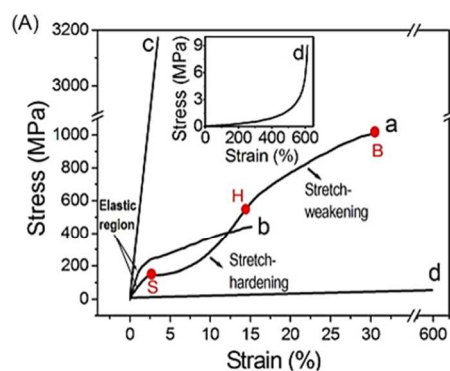


Fig. 32(A) Comparison between typical stress-strain curves of silk fibers and spider *N. pilipes* (by forced silking at $10 \text{ mm}\cdot\text{s}^{-1}$, curve a) draglines and silkworm cocoon *B. mori* (curve b). Spider draglines exhibit a characteristic strain-hardening feature in the non-linear region of the stress-strain curve. (B) A schematic model demonstrating how the silkworm and spider dragline fibers respond when they are subjected to stretching. There are two β -components in the alanine-rich regions of spider dragline silk: β -crystallites and intra-molecular β -sheets. The intra-molecular β -sheets are mainly responsible for the extensibility while the β -crystallites and the orientation and density are responsible for the toughness of silk fibers. (C) Effect of tensile deformations on the β -crystallinity of spider *N. pilipes* dragline fibers. (A) and (C) are Reprinted with permission from Ref. ⁹². Copyright 2011, Wiley-VCH.

The X-ray data of deformed fibers show that the β -crystallinity of the dragline starts declining once a spider dragline is stretched beyond point H.⁹² On the other hand, silkworm silk fibers have far fewer intra-molecular β -sheets in the amorphous region. Therefore it is less extensible and only exhibits strain-weakening after yield point. The property of strain-hardening of spider draglines plays a key role in supporting a suspended spider. In the case of a spider escaping from a predator by abseiling, the soft spider dragline can effectively buffer the impact force with its gradually hardening property.¹⁰² The stress-strain profile of the spider dragline shows that the *J*-shaped strain-hardening curve accounts for a very large extension, enabling quick absorption of tremendous energy at low applied stress, so draglines can facilitate safe and gentle falls.

6.3. Hierarchical Breaking Mechanism

6.3.1 Role of Bundle Structure in Silk Fiber Toughness

The breaking stress, or the toughness, of two types of silk fibers can be explained according to the hierarchical structures as shown by Figs. 2B-b, 31 and 33(B). As revealed by Fig. 30, silk fibers correspond to crystal networks (nano fibrils) and domain networks (fibres) defined by Fig. 3, respectively: the nano-fibrils are to molecular networks where β -crystallites are the nodes of the networks and molecular chains linking the nodes; a silk fiber as a bundle of twisted nano-fibrils (Fig. 32(B)), which are interlocked by adjacent ones so that they cannot slip freely. This implies that the interactions between the adjacent domains are very strong/infinite (Fig. 3(B)-(b)).

Within this framework, a twisted fibril can be regarded in the form of periodically repeating segments (Fig. 33(A)). Therefore, the breakage of fibrils happens at the maximum loading of these associated “segments”. The breakage of a fibril bundle is initiated by the fracture of the weakest segments,^{86, 94} indicate that these “rough” fibrils can effectively avoid mutually slipping even when the silk fibers are approaching the breaking points.¹⁰³ Regarding the fact that silk fibers are very long, the interactions between adjacent nanofibrils (crystal networks) in the bundles (domain networks) are very strong (Fig. 33(B)-(a), Nonslipping Fibril Bundle (N-NFB)). This implies that the interactions between domains are very strong (Fig. 31(B)-(b)) In stretching, the breaking of fibrous bundle will form nano cracks in silk fiber (Fig. 33(B)-(a)-(ii)), and disperse at different cross sections of the fiber. This will prevent the catastrophic fracture of the fibril bundle. The fiber breakage occurs only if all the fibrils in a cross section of the fiber are all broken (Fig. 33(B)-(a)-(iv)). It follows that the extra stress caused by fractured segments can be distributed uniformly among the uncracked

segments of the silk nano fibril bundle along the same cross section. This is what was observed in practice (Fig. 33(B)-(a)-(v)). Then, the breaking of such a fiber (bundle) can be described as follows:¹⁰⁴ the cracks are accumulating gradually in the fibril bundle, with the extra stress equally shared among the unbroken segments within the same cross section; if enough cracks accumulate at one cross section of the fiber, the catastrophic breakage across the fibril bundle occurs. For the aforementioned structure, there are three significant structural effects on the strength of silks: (1) the molecular networks inside nano-fibril, with β -crystallites as the nodes, which can reinforce the connection between fibroin molecules,¹⁰⁵ (2) the periodic twisted segmental morphology of fibrils which prevents the slipping between adjacent fibrils, (3) the fibril bundle structure together with the non-slipping feature between fibrils makes the extra stress equally shared among the unbroken segments.

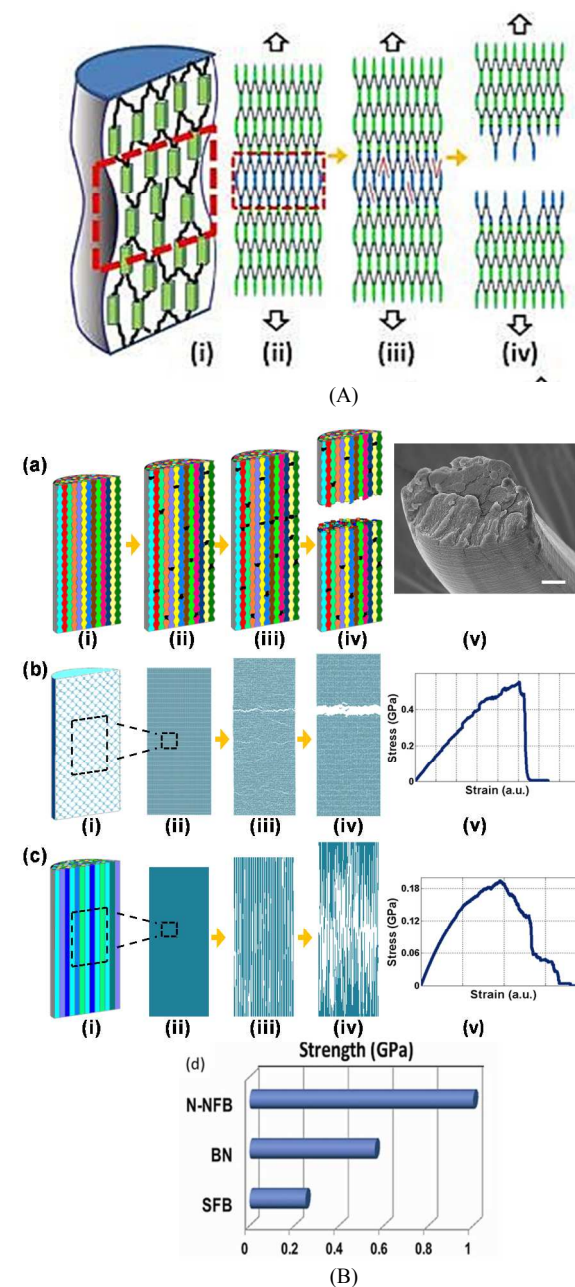


Fig. 33 (A). Schematic illustration of the segmental structure of nano-fibrils. (B). (a-i-iv) Illustration of the breaking mechanism of Network - Nonslipping Fibril Bundle (N-NFB) at the nano-fibril bundle scale; (a-v) SEM image of the transverse cross section of a *B. mori* silkworm silk fiber after its breakage upon stretching (scale bar: 2 μm). (b-i) schematic illustration of the bulk network (BN) model; (b-ii-iv) the scenarios showing the breakage of BN by simulation; (b-v) typical stress strain curve of BN model; (c-i) schematic illustration of the Network - Slippery Fibril Bundle (SFB) model; (b-ii-iv) the scenarios showing breakage of SFB by simulation; (b-v) typical stress strain curve of SFB model. In comparison with BN, the nano-fibrillar structure in N-NFB can inhibit the transverse growth of the crack; and in comparison with SFB, the friction between nano-fibrils in N-NFB can prevent the longitudinal growth of the crack. These are the structural advantages of N-NFB which make silk fibers strong. (d) Comparison of the breaking stresses of silk fibers predicted by N-NFB, SFB and BN model. Notice that the strength difference between N-NFB and BN in B-(d) can be correlated in some way to the dependence of G' on the domain density Fig. 9c, where G' increases with the domain density. Reprinted with permission from Ref. ⁹⁴. Copyright 2014 Royal Society of Chemistry.

The advantage of the hierarchical structure of N-NFB silk fibers in toughening the silk fibers can be further demonstrated by comparing the above structure (the N-NFB structure or Fig. 33(B)-(d)) with other two structures. One is the Slippery Fibril Bundle (SFB) structure (Fig. 33(B)-(c) or Fig. 3B-a) and the other is Bulk Network (BN) structure (Fig. 31(B)-(b)). The SFB model assumes that the nanofibrils are cylindrical and can slip freely (there is no frictions between them). The BN structure does not have the fibril bundle structure and the molecular-crystallite structure is extended to the whole fibers.

In the BN structure, a silk fiber is considered to be a bulk molecular network without fibril bundle structure (Fig. 33B-(b)-(i)). The network here is the same as the molecular network in a segment of fibril in the nano-fibril structure (Fig. 33(A)). The snapshots of the bulk network (BN) upon the stretching until breakage in the simulations and the corresponding mechanical behaviour are displayed in Fig. 31(B)-(b)-ii-iv and 31(B)-(b)-v, respectively. In this case, the breakage of BN behaves similarly with brittle materials, where the fracture occurs as the catastrophic growth of cracks.¹⁰⁶ According to Griffith's fracture theory, the extra stress caused by a crack is concentrated around the crack, especially at the transverse boundary of the crack (Fig. 33(B)-(b)), while in the N-NFB structure, the extra stress will be redistributed uniformly in the cross section of the fiber which contains cracks (Fig. 33(B)-b). In the BN structure, the concentration of the extra stress can promote the propagation of the cracks, causing the split of the materials.¹⁰⁷ Hence, such fibers based on this model will obtain the strength of 0.56 ± 0.04 GPa, much weaker than 1.00 ± 0.02 GPa obtained from the HN structure.

In the SFB structure, a bundle of nano-fibrils were stretched gradually. The snapshots of the simulations of stretching SFB to Breakage are displayed in Fig. 33(B)-(c)-ii-iv. As each nano-fibril takes the load independently, the breakage of a nano-fibril occurs at its weakest position. The breakage will first start from the weakest nano fibrils and will accelerate the breakage of the remaining fibrils as the total load will add to the unbroken fibrils. This will lead to the breakage of the entire fiber. Therefore, a SFB like fiber will be the weakest among the three types and breaks at 0.25 ± 0.03 GPa. The resulting stress-strain curve is plotted in Fig. 33(B)-(c)-(v). It follows that a gradual breakage occurs at the breaking point, it behaves very similar to ductile materials, whose deformation is

intermediated by localized shear at the nanoscale.¹⁰⁸ However, in contrast, the silk fibers always break abruptly in practice.

In comparison, the breaking stresses according to the N-NFB, BN and SFB structures are given in Fig. 33(B)-(d). The plot indicates that the HN structure, corresponding to Fig. 3B-b, gives the highest breaking stress. The observed non-slipping feature and the fibril bundle structure do have their implication in the strength enhancement of silk fibers. In the BN structure, a crack can develop along the transverse direction easily, due to its single network structure. However, in both the N-NFB and the SFB structures, the boundaries of the fibrils can physically terminate the growth of the cracks across the fibers, and the surviving nano-fibrils can redistribute the extra stress resulted from the broken fibrils uniformly. On the other hand, in the SFB structure, the cracks can propagate in the direction of the fiber axis without any impediment. Nevertheless, in the case of N-NFB, the inter-fibrillar friction arising from the adjacent twisted nano-fibrils will prevent the crack propagation of this type. In other words, the non-slipping fibril bundle structure shows a crack-stopping property in blocking the propagation of cracks in both the transverse and the longitudinal directions.

Based on the discussion above, the synergy between the network structure at the nano-fibril scale and the fibril bundle structure at the fiber scale can be explained as follows: At the crystal network level, the fibrils are the molecule- β -crystallite networks, where β -crystallites serve as nodes in the molecular network (c.f. Fig. 33(A)). If we take it as the reference that the fibers have only one level of the structure, the molecule- β -crystallite network, the domain structure exerts a significant impact on the mechanical properties of silk fibers. In case of the SFB structure (Fig. 33(B)-(b) or Fig. 3B-a), no interaction occurs among the adjacent fibrils (networks). Thus, the silk fiber strength deteriorates, and the breaking stress becomes weaker than the BN structure. On the other hand, the N-NFB structure (Fig. 33(B)-(a)) makes the fibril-fibril interactions strong. This greatly enhances the strength of the silk fibers. In other words, the twisted nano fibrils lead to stronger domain (fibril) – domain (fibril) interactions. We notice that the interlock among the adjacent nano fibrils in the nano fibril bundle serves as the crack-stopper, which restricts the propagation of cracks. This consequently strengthens the silk fibers significantly.

6.3.2. Regenerated Silk Protein Derivatives and Silk Fibers: Mechanical Performance vs Hierarchical Structure

As mentioned above, regenerated silk protein derivatives refer to the films, sponges, hydrogels, etc. from regenerated silk proteins. Recent AFM and SEM experiments reveal that in the solidification process of regenerated silk fibroin (RSF) solutions, silk fibroin molecules self assemble into nanofibrils of the diameter as revealed by Fig. 31b. Representative SEM images of the nano fibril networks from freeze-dried regenerated silk fibroin sponges are shown in **Fig. 34a,b**. The fibril networks consist of nanofibers of ~ 30 nm in diameter. **Fig. 34c** shows the wide angle X-ray scattering (WAXS) patterns of the β -crystallites from a regenerated silk fibroin sponge. It follows that all the structural parameters of regenerated silkworm silk fibrils, i.e. the crystallinity, the average β -crystal size, and the β -component ratios within regenerated silk fibrils, are confirmed to be close to the natural silk fibers apart from the orientation of β -crystallites (the results to be published).

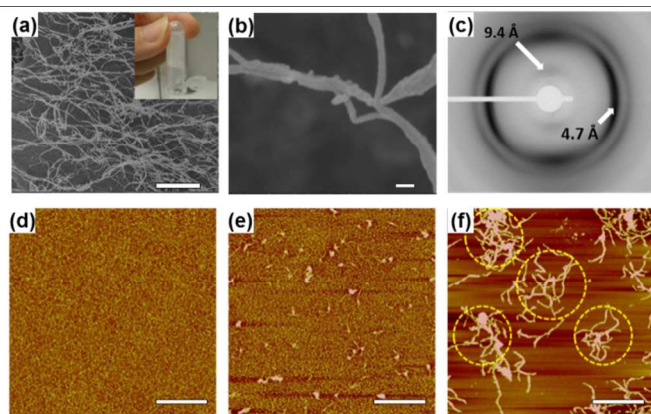


Fig. 34. a, b) Representative SEM images of freeze-dried regenerated silk fibroin (RSF) sponges (inset: a hydrogel formed after sonication with the self-supporting behavior); c) 2D WAXS pattern of silk fibrils. d-f) AFM images of RSF solutions (wt/v 0.04%) at different gelation stages: d) before ultrasonication, e) right after ultrasonication, and f) 30 minutes after ultrasonication. The ultrasonication time was 30 seconds. Scale bars: a) 1 μm , b) 100 nm, d-f) 500 nm. Reprinted with permission from Ref. ⁸⁶. Copyright 2015 Wiley-VCH.

The above results display a fact: both silk fibres and silk protein derivatives have similar structures apart from the domain (fibril-fibril) networks. The domain networks of silk protein derivatives silk fibres correspond to the case of Fig. 3B-(a) or the SFB structure in Fig.33(B)-(d) while and those of silk fibres correspond to the case of Fig. 3B-(b) or the N-NFB structure in Fig.33(B)-(d). In addition to the strong interaction, the nano fibrils in the silk fibres are well aligned whereas the fibrils in regenerated silk fibroin films, sponges or hydrogels are much less ordered or in the form of random coils. In other words, the domains in the domain networks of silk fibres are much better ordered than regenerated silk fibroin films, sponges or hydrogels. As a consequence, spider or silkworm silk fibers are much strong (breaking stress: from a few hundreds to > 1000 GPa) than regenerated silk fibroin films or sponges (breaking stress: a few tens Gpa; the results to be published).

6.3.3 Molecular β -Crystallite Network Structure of Nano fibrils and Silk Fiber Breaking Limit

Apart from the inter fibrillar or bundle structure, the structure of molecular- β nano crystallite networks in fibrils plays a crucial role in the toughness (breaking stress) of both spider silk fibers and silkworm silk fibers. According to the data f presented in Table 4,⁹² spider silk fibers have higher f 's than silkworm silk fibers. This corresponds to the fact that spider dragline silk fibers have high breaking stress than silkworm silk fibers. To examine systematically the impact of the correlation length and ordering of crystal networks on the mechanical performance of the two types of silk fibres, one can change the reeling speed of silking (*Supplemental Info*) to acquire the correlation between the breaking stress and strain of silk fibers and the crystal network structure of silk fibers. According to Liu *et al.*,^{92, 94} f can be further enhanced by faster reeling/spinning of both spider and silkworm silk fibers.¹⁰⁹ It is surprising to see from Fig. 35(a) that the breaking stress of both spider dragline silk and silkworm silk fibers increases with f unambiguously in the same fitting curve after eliminating the influence of other factors. This implies that the orientation of nano crystallites in the networks of silk fibrils exerts a predominant influence on the breaking stress of all types of silk fibrous materials.

On the other hand, we notice that the crystallinity of silkworm silk fibers is higher than spider dragline silk fibers (Table 4). The arising question comes as to why spider dragline silk fibers are stronger than silkworm silk fibers? The analysis based on the HN structure (Fig.33) indicates that in addition to f , the breaking stress can be correlated to the number of the β -crystallites n_β within the cross section of a nano-fibril (c.f. Fig. 35(d)),⁹⁴ and the effective loading area A of a peptide chain in the β -crystallites, where A can be defined as

$$A = \frac{\text{Cross Sectional Area of the fibril}}{\text{Number of Peptide Chain in One Crystallite} \times n_\beta} \quad (20)$$

It follows that increasing n_β gives rise to somewhat increase in the breaking stress of silk fibers (Fig. 35(b)) and the breaking stresses of the silk fibres decrease while A increases (Fig. 35(c)).

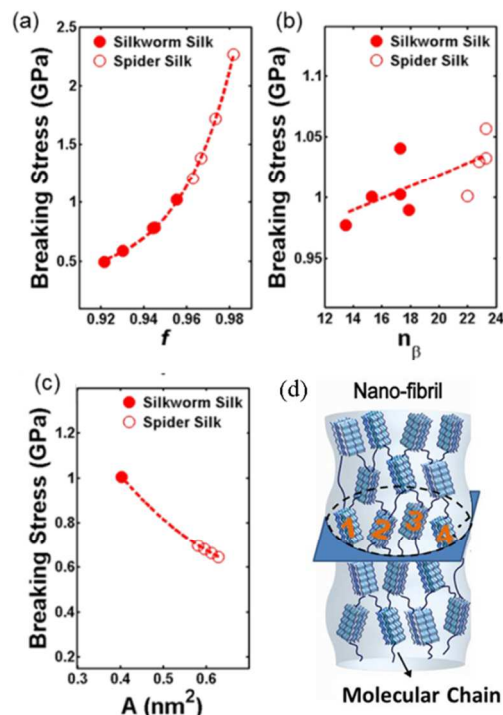


Fig. 35. The influence of three structural parameters (a) f , (b) n_β , (c) A on the breaking stress of the segments at the nano-fibril scale. At keeping other parameters constant, the breaking stress of both spider dragline silk and silkworm silk fibers increases exponentially with f , or increases linearly, or decreases with A . Here, $A \sim \xi^2$. The striking point is that both spider silk and silkworm silks can be fitted by the same curves, meaning that the strength of the two types of fibers is governed by the similar structures. Reprinted with permission from Ref. ⁹⁴. Copyright 2014 Royal Society of Chemistry. (d) Schema for n_β and A , n_β is the number of crystallites at the cross section of a fibril. A is defined as the effective loading area of a peptide chain in the β -crystallites.

Within the framework of hierarchical network structures, both spider silkworm silk fibers consist of essentially the same structural components: the crystal networks of molecular-nano β -crystallites in nano fibrils and the nano fibrils (or bundles) networks. This is why the key structural parameters of the both species can be fitted by the same curves. In this concern, the twisting of silk fibrils leads to the strong retardation of mutual slip between adjacent fibrils, which

significantly enhances the breaking stress of silk fibres. At the nano-fibril level, a better alignment of nano β -crystallites, a larger number of β -crystallites at one cross section of a nano-fibril and a smaller effective loading area of a peptide chain in β -crystallites will eventually give rise to stronger silk fibers.

We notice there have been continuous efforts in acquiring stronger silkworm silks fibers by genetically modifying the amino acid sequence of silk fibroin. Such efforts are to allow transgenic silkworms to spin “super” silk fibers having the partial spidroin sequences so as to acquire fibers as strong as spider dragline fibers¹¹⁰. The results depicted by Fig.35 indicate that the key structural parameters, i.e. f , A , n_{β} etc., that determine the toughness of silk fibers are decided by both the amino acid sequence or the primary structure of silk proteins, and the reeling speed of silking process. Based on the facts that the natural reeling speed of silkworms is 4 mm/sec and that of spiders is about 15–20mm/sec,⁵³ and the fact that f , A , n_{β} etc. to a large extent are determined by reeling speed, even if silkworms could spin the silk fibers of the spidroin amino acid sequence, the breaking stress is never going to match that of natural spider dragline fibers due to the much lower reeling speed of the silkworms. In other words, the dream of naturally spinning “stronger spider dragline fibers” by transgenic silkworms is very unlikely to realize in the natural spinning process by silkworms unless the nano β -network structure is completely modified.

7. Summary and Outlook

While crystallization has been regarded as one of the most crucial processes in science and engineering for centuries, the latest development in materials sciences requires the further application of the crystallization knowledge beyond the classic domain to the “unrelated” area of soft matter. Although crystal networks become the “backbones” of mesoscopic/soft materials, the structure of crystal networks in general plays an irreplaceable role in the performance and critical behaviour of materials. In other words, the ability to control the hierarchical structure of crystal networks will enable us to acquire the capability to design materials with some particular functions of mesoscopic/soft materials. This broadens the application of the concepts and knowledge of crystallization. On the other hand, we notice that in distinct with the conventional crystallization, the association of crystals in the form of networks become one of particular relevance of interests in the mesoscale. In this context, the form of hierarchical structures becomes inevitable: the occurrence of hierarchical structures is a kinetically favoured event, and will boost up the macroscopic performance of materials in some cases (i.e. spider silk fibers). In the framework of crystal networks, the key structural parameters that characterize crystal networks, and the corresponding macroscopic performance of mesoscopic materials are among the main concerns. In this regard, a comprehensive summary on the definition and classification of various crystal networks and different levels was given. In particular, the four different structural parameters, namely, *topology*, *correlation length*, *ordering* and *structural interaction* allow for the first time the quantitative characterization of the correlation between the hierarchical network structure versus the function and performance of soft matter.

Concerning the formation mechanism, we casted an overview on main mechanisms of conventional crystallization i.e. nucleation, the Birth and Spread and the Spiral Growth mechanisms. These were further extended to the description of crystal network formation. Moreover, it was identified that there are four typical pathways, namely, *one-step*, *two-step*, *mixed mode of assembly* and *foreign molecule mediated assembly* in the network construction.

We notice that the fundamental knowledge acquired will only make sense if it can be applied to engineer or functionalize materials in effective and controllable manners. In this regard, the elegant engineering of materials should be based on a decent understanding on the formation of crystal networks and the correlation between the structure and the performance of materials, and the formation kinetics. To achieve some particular performance, the engineering of soft materials can be implemented by mesoscopic crystal network (re)construction. This can be achieved by various means, i.e. thermal, participate, chemical, sonication stimuli etc, across different levels of structures.

Spider dragline silk fibers turn out to be a typical example of high performance soft materials. It was found that the knowledge of hierarchical crystal networks and the four structural parameters should be able to decode the structural information leading to the unusual performance-structure correlation. Within this framework, both spider and silkworm silk fibers consist of a bundle of twisted nano-fibrils, leading to strong fibril-fibril (crystal network) interactions. This gives rise to the significant enhancement in the toughness of fibers. On the other hand, the ordering, and the correlation length of β -nano crystallites in the molecular crystallite networks at the nano-fibril level have a direct impact on the breaking stress of silk fibers. The fact that a better alignment of β -crystallites, a larger number of β -crystallites within a cross section of a nano-fibril and a smaller effective loading area of a peptide chain will correlatively lead to stronger silk fibers can be explained and predicted within the framework of the crystal network model. Evidently, the knowledge obtained will shed light on how to obtain ultra-performance of soft materials from the structural point of view.

This paper provides a comprehensive overview on how to examine the “non-crystalline” matter by “crystalline eyes”. On one hand, this will open up a new dimension of research for the crystallization community. The theories of crystallization can be further developed to resolve some key issues and to address the doubts arising from the soft materials research community. On the other hand, such efforts also produce new research topics for people from the crystallization community to work on. More specifically, the quantitative description for crystal networks requires more effort and continuous attention. Furthermore, the knowledge of crystal networks should be translated in such a way that can facilitate the functionalization, and rational design of mesoscopic materials in a more controllable manner.

Acknowledgements

This work is financially supported by AcRF Tier 1(R-144-000-348-112), National Nature Science Foundation (Nos. 21404087, U1405226), and the 1000 Talents Program from Xiamen University.

Notes and references

^a Research Institute for Biomimetics and Soft Matter, Xiamen University, Xiamen, 361005, China. E-mail address: phyluxy@nus.edu.sg (X. Y. Liu)
^b Department of Physics, National University of Singapore, 2 Science Drive 3, Singapore, 117542, Singapore.

† Electronic Supplementary Information (ESI) available: [Two videos of the reeling process of silkworm and spider.].

1. a) G. Gibbs, *Collected Works. Vol. I: Thermodynamics Longmans and Green*, Longmans, 1928; b) L. Farkas, *Z. Phys. Chem.*, 1927, **125**, 236-242.
2. a) R. Becker and W. Döring, *Annalen der Physik*, 1935, **416**, 719-752; b) Y. B. Zeldovich, *Acta physicochim. URSS*, 1943, **18**, 1-22.
3. J. Hemminger, G. Crabtree and J. Sarrao, *A Report from the Basic Energy Sciences Advisory Committee, Tech. Rep*, 2012, 1601-1606.

4. J. L. Li and X. Y. Liu, in *Soft Fibrillar Materials: fabrication and applications*, ed. J. L. L. X. Y. Liu, Wiley-VCH Verlag GmbH & Co. KGaA, Weinheim, Germany, 2013, pp. 163-182.
5. B. Lewis and J. C. Anderson, *Nucleation and growth of thin films*, Academic Press New York, 1978.
6. a) J.-L. Li, B. Yuan, X.-Y. Liu, R.-Y. Wang and X.-G. Wang, *Soft Matt.*, 2013, **9**, 435; b) F. Vollrath and D. P. Knight, *Nature*, 2001, **410**, 541-548; c) D. Heberer, A. Keller and V. Percec, *J. Polym. Sci. Pol. Phys.*, 1995, **33**, 1877-1894; d) J. Y. Xiong, X. Y. Liu, J. L. Li and M. W. Vallon, *J. Phys. Chem. B*, 2007, **111**, 5558-5563.
7. M. Perneti, K. van Malssen, D. Kalnin and E. Flöter, *Food Hydrocolloids*, 2007, **21**, 855-861.
8. a) P. F. C. Lim, X. Y. Liu, L. Kang, P. C. L. Ho, Y. W. Chan and S. Y. Chan, *Int. J. Pharm.*, 2006, **311**, 157-164; b) L. Kang, X. Liu, P. Sawant, P. Ho, Y. Chan and S. Chan, *J. Control. Release*, 2005, **106**, 88-98.
9. a) H. Wang, X. Y. Liu, Y. J. Chuah, J. C. H. Goh, J. L. Li and H. Xu, *Chem. Commun.*, 2013, **49**, 1431-1433; b) B. Kundu, R. Rajkhowa, S. C. Kundu and X. Wang, *Adv. Drug Del. Rev.*, 2013, **65**, 457-470.
10. A. Ajayaghosh, V. K. Praveen and C. Vijayakumar, *Chem. Soc. Rev.*, 2008, **37**, 109-122.
11. K. K. Kartha, S. S. Babu, S. Srinivasan and A. Ajayaghosh, *J. Am. Chem. Soc.*, 2012, **134**, 4834-4841.
12. K. J. van Bommel, A. Friggeri and S. Shinkai, *Angew. Chem. Int. Ed.*, 2003, **42**, 980-999.
13. E. Carretti, M. Bonini, L. Dei, B. H. Berrie, L. V. Angelova, P. Baglioni and R. G. Weiss, *Acc. Chem. Res.*, 2010, **43**, 751-760.
14. a) S.-M. Lee, E. Pippel, U. Gosele, C. Dresbach, Y. Qin, C. V. Chandran, T. Brauniger, G. Hause and M. Knez, *Science*, 2009, **324**, 488-492; b) N. Becker, E. Oroudjev, S. Mutz, J. P. Cleveland, P. K. Hansma, C. Y. Hayashi, D. E. Makarov and H. G. Hansma, *Nat. Mater.*, 2003, **2**, 278-283.
15. S.-T. Dictionary, The McGraw-Hill Companies, Inc., New York, 2003.
16. R. Albert and A.-L. Barabási, *Rev. Mod. Phys.*, 2002, **74**, 47.
17. G. Xu, L. Gong, Z. Yang and X. Liu, *Soft Matt.*, 2014, **10**, 2116-2123.
18. a) X. Y. Liu and P. D. Sawant, *Appl. Phys. Lett.*, 2001, **79**, 3518-3520; b) X. Y. Liu and P. D. Sawant, *Chemphyschem*, 2002, **3**, 374-377; c) X. Y. Liu and P. D. Sawant, *Adv. Mater.*, 2002, **14**, 421-426; d) Y. Liu, R.-Y. Wang, J.-L. Li, B. Yuan, M. Han, P. Wang and X.-Y. Liu, *CrystEngComm*, 2014, **16**, 5402-5408; e) X. Huang, P. Terech, S. R. Raghavan and R. G. Weiss, *J. Am. Chem. Soc.*, 2005, **127**, 4336-4344; f) K. L. Caran, D. C. Lee and R. G. Weiss, in *Soft Fibrillar Materials: fabrication and applications*, ed. J. L. L. X. Y. Liu, Wiley-VCH Verlag GmbH & Co. KGaA, Weinheim, Germany, 2013, pp. 3-75; g) J. L. Li and X. Y. Liu, in *Soft Fibrillar Materials: fabrication and applications*, ed. J. L. L. X. Y. Liu, Wiley-VCH Verlag GmbH & Co. KGaA, Weinheim, Germany, 2013, pp. 77-114.
19. X. Y. Liu and P. D. Sawant, *Adv. Mater.*, 2002, **14**, 421-426.
20. R. Lam, L. Quaroni, T. Pederson and M. A. Rogers, *Soft Matt.*, 2010, **6**, 404-408.
21. H. C. Wang, X. Y. Liu, W. L. Lu, A. Chang, Q. Zhang, B. C. Goh and H. S. Lee, *Eur. J. Pharm. Biopharm.*, 2006, **62**, 44-51.
22. a) A. A. Chernov, *Modern crystallography*, Springer, 1984; b) B. Mutaftschiev, ed. D. T. J. Hurler, North Holland, Amsterdam, 1993, pp. 189-245.
23. X.-Y. Liu, *J. Phys. Chem. B*, 2001, **105**, 11550-11558.
24. S. Tang, X. Y. Liu and C. S. Strom, *Adv. Funct. Mater.*, 2009, **19**, 2252-2259.
25. M. A. Rogers and A. G. Marangoni, *Cryst. Growth Des.*, 2008, **8**, 4596-4601.
26. X. Y. Liu and Y. Y. Diao, in *Bioinspiration: From Nano to Micro Scales*, ed. X. Y. Liu, Springer, New York, 2012, p. 249.
27. H. Jiang, X.-Y. Liu, C. T. Lim and C. Y. Hsu, *Appl. Phys. Lett.*, 2005, **86**, 163901.
28. X. Y. Liu, in *Low Molecular Mass Gelators: Design, Self-Assembly, Function*, ed. F. Fréché, Springer, Berlin, 2005, vol. 256, pp. 1-37.
29. J.-Y. Xiong, X.-Y. Liu, J.-L. Li and M. W. Vallon, *J. Phys. Chem. B*, 2007, **111**, 5558-5563.
30. J.-L. Li, X.-Y. Liu, X.-G. Wang and R.-Y. Wang, *Langmuir*, 2011, **27**, 7820-7827.
31. P. D. Sawant and X.-Y. Liu, *Chem. Mater.*, 2002, **14**, 3793-3798.
32. X. Y. Liu and P. D. Sawant, *Angew. Chem. Int. Ed.*, 2002, **114**, 3793-3797.
33. P. Bennema, X. Y. Liu, K. Lewtas, R. Tack, J. Rijpkema and K. Roberts, *J. Cryst. Growth*, 1992, **121**, 679-696.
34. a) J. A. Foster, M.-O. M. Piepenbrock, G. O. Lloyd, N. Clarke, J. A. Howard and J. W. Steed, *Nat. Chem.*, 2010, **2**, 1037-1043; b) P. F. C. Lim, X. Y. Liu, L. Kang, P. C. L. Ho and S. Y. Chan, *Int. J. Pharm.*, 2008, **358**, 102-107; c) S. B. W. j. Yan, L. F. Kang, in *Soft Fibrillar Materials: fabrication and applications*, ed. J. L. L. X. Y. Liu, Wiley-VCH Verlag GmbH Co. KGaA, Weinheim, Germany, 2013, pp. 129-162; d) F. G. Omenetto and D. L. Kaplan, *Science*, 2010, **329**, 528-531; e) D. N. Rockwood, R. C. Preda, T. Yücel, X. Wang, M. L. Lovett and D. L. Kaplan, *Nat. Protoc.*, 2011, **6**, 1612-1631.
35. X. Y. Liu, P. D. Sawant, W. B. Tan, I. Noor, C. Pramesti and B. Chen, *J. Am. Chem. Soc.*, 2002, **124**, 15055-15063.
36. a) M. Ye, X. Xin, C. Lin and Z. Lin, *Nano Lett.*, 2011, **11**, 3214-3220; b) M. Ye, D. Zheng, M. Lv, C. Chen, C. Lin and Z. Lin, *Adv. Mater.*, 2013, **25**, 3039-3044; c) M. Ye, H. Y. Liu, C. Lin and Z. Lin, *Small*, 2013, **9**, 312-321; d) M. Ye, C. Chen, M. Lv, D. Zheng, W. Guo and C. Lin, *Nanoscale*, 2013, **5**, 6577-6583.
37. X. Y. Liu, *Bioinspiration: From Nano to Micro Scales*, Springer, 2012.
38. X. D. Zhao, H. M. Fan, X. Y. Liu, H. Pan and H. Y. Xu, *Langmuir*, 2011, **27**, 3224-3228.
39. Ning Du, Guoyang William Toh and X. Y. Liu, in *Bioinspiration: From Nano to Micro Scales*, ed. X. Y. Liu, Springer, New York, 2012, pp. 57-106.
40. H. Jiang and X.-Y. Liu, *J. Biol. Chem.*, 2004, **279**, 41286-41293.
41. a) X. Y. Liu and S. W. Lim, *J. Am. Chem. Soc.*, 2003, **125**, 888-895; b) H. Jiang, X.-Y. Liu, G. Zhang and Y. Li, *J. Biol. Chem.*, 2005, **280**, 42061-42066; c) J. Liu, H. Jiang and X.-Y. Liu, *J. Phys. Chem. B*, 2006, **110**, 9085-9089.
42. J. H. Shi, X. Y. Liu, J. L. Li, C. S. Strom and H. Y. Xu, *J. Phys. Chem. B*, 2009, **113**, 4549-4554.
43. Y. Y. Diao, X. Y. Liu, G. W. Toh, L. Shi and J. Zi, *Adv. Funct. Mater.*, 2013, **23**, 5373-5380.
44. a) Y. Y. Diao and X. Y. Liu, *Adv. Funct. Mater.*, 2012, **22**, 1354-1375; b) J. Zi, B. Q. Dong, T. R. Zhan and X. H. Liu, in *Bioinspiration: From Nano to Micro Scales*, ed. X. Y. Liu, Springer, New York, 2012, pp. 221-276.
45. a) B. Yuan, J.-L. Li, X. Y. Liu, Y.-Q. Ma and Y. J. Wang, *Soft Matt.*, 2012, **8**, 5187-5193; b) B. Yuan, J.-L. Li, X. Y. Liu, Y.-Q. Ma and H.-Y. Xu, *Chem. Commun.*, 2011, **47**, 2793-2795; c) B. Yuan, X.-Y. Liu, J.-L. Li and H.-Y. Xu, *Soft Matt.*, 2011, **7**, 1708-1713.
46. a) J. W. Gibbs, *Trans. Connect. Acad. Sci.*, 1876, **3**, 108-248; b) J. W. Gibbs, *Trans. Connect. Acad. Sci.*, 1878, 343-524; c) T. H. Zhang and X. Y. Liu, *Angew. Chem. Int. Ed.*, 2009, **48**, 1308-1312; d) T. H. Zhang and X. Y. Liu, *Chem. Soc. Rev.*, 2014, **43**, 2324-2347; e) X.-Y. Liu, P. Bennema and J. Van der Eerden, *Nature*, 1992, **356**, 778-780.
47. X. Liu, *Langmuir*, 2000, **16**, 7337-7345.
48. a) X. Y. Liu, in *Advances in Crystal Growth Research*, eds. K. Sato, Y. Furukawa and K. Nakajima, ELSEVIER SCIENCE, B.V., Amsterdam, 2001, pp. 42-61; b) K.-Q. Zhang and X. Y. Liu, *Nature*, 2004, **429**, 739-743.
49. a) C. S. Strom, X. Y. Liu and Z. C. Jia, *J. Am. Chem. Soc.*, 2005, **127**, 428-440; b) X. Y. Liu, in *Nanoscale structure and assembly at solid-fluid interfaces*, ed. J. J. D. X. Y. Liu, Springer, London, 2004, vol. I, pp. 109-175.
50. T. H. Zhang and X. Y. Liu, *J. Am. Chem. Soc.*, 2007, **129**, 13520-13526.
51. a) X. Y. Liu, in *Advances in Crystal Growth Research*, ed. K. N. K. Sato, Y. Furukawa, Elsevier Science, Amsterdam, The Netherlands, 2001, pp. 42-61; b) X. Liu, *J. Chem. Phys.*, 1999, **111**, 1628-1635; c) X. Liu, K. Maiwa and K. Tsukamoto, *J. Chem. Phys.*, 1997, **106**, 1870-1879.
52. X. Y. Liu, *J. Chem. Phys.*, 1999, **111**, 1628-1635.
53. N. Du, X. Y. Liu, J. Narayanan, L. Li, M. L. M. Lim and D. Li, *Biophys. J.*, 2006, **91**, 4528-4535.
54. W. Z. Ostwald, *Phys. Chem.*, 1879, **22**, 289-330.
55. a) I. M. Weiss, N. Tuross, L. Addadi and S. Weiner, *J. Exp. Zool.*, 2002, **293**, 478-491; b) L. Addadi, S. Raz and S. Weiner, *Adv. Mater.*, 2003, **15**, 959-970.
56. a) L. Addadi and S. Weiner, *Angew. Chem. Int. Ed.*, 1992, **31**, 153-169; b) S. E. Wolf, I. Lieberwirth, F. Natalio, J.-F. Bardeau, N. Delorme, F. Emmerling, R. Barrea, M. Kappl and F. Marin, *Faraday Discuss.*, 2012, **159**, 433-448.

57. D. Kashchiev, P. G. Vekilov and A. B. Kolomeisky, *J. Chem. Phys.*, 2005, **122**, 244706.
58. Haihua Pan, Xiang Yang Liu, Ruikang Tang and H. Y. Xu, *Chem. Commun.*, 2010, **46**, 7415-7417.
59. K. Sugiyasu, N. Fujita and S. Shinkai, *Angew. Chem. Int. Ed.*, 2004, **116**, 1249-1253.
60. F. Frank, *Discuss. Faraday Soc.*, 1949, **5**, 48-54.
61. W.-K. Burton, N. Cabrera and F. Frank, *Philosophical Transactions of the Royal Society of London. Series A, Mathematical and Physical Sciences*, 1951, 299-358.
62. P. Bennema, *J. Cryst. Growth*, 1984, **69**, 182-197.
63. a) X. Liu, E. Boek, W. Briels and P. Bennema, *J. Chem. Phys.*, 1995, **103**, 3747-3754; b) X. Liu, E. Boek, W. Briels and P. Bennema, *Nature*, 1995, **374**, 342-345.
64. a) H. Cölfen and M. Antonietti, *Angew. Chem. Int. Ed.*, 2005, **44**, 5576-5591; b) V. M. Yuwono, N. D. Burrows, J. A. Soltis and R. L. Penn, *J. Am. Chem. Soc.*, 2010, **132**, 2163-2165.
65. X. Zhang, D. Görl, V. Stepanenko and F. Würthner, *Angew. Chem. Int. Ed.*, 2014, **53**, 1270-1274.
66. Z. Bian, T. Tachikawa, P. Zhang, M. Fujitsuka and T. Majima, *Nat. Commun.*, 2014, **5**.
67. Z. Wang, G. Ma and X. Y. Liu, *J. Phys. Chem. B*, 2009, **113**, 16393-16399.
68. H. Zhai, Y. Quan, L. Li, X.-Y. Liu, X. Xu and R. Tang, *Nanoscale*, 2013, **5**, 3006-3012.
69. a) J. Liu, *Adv. Funct. Mater.*, 2010, **20**, 21; b) J. L. Li, X. Y. Liu, C. S. Strom and J. Y. Xiong, *Adv. Mater.*, 2006, **18**, 2574-2578.
70. N. Vandewalle and M. Ausloos, *Phys. Rev. E*, 1997, **55**, 94-98.
71. R. Lam, L. Quaroni, T. Pedersen and M. A. Rogers, *Soft Matt.*, 2010, **6**, 404-408.
72. a) J.-Y. Xiong, J. Narayanan, X.-Y. Liu, T. K. Chong, S. B. Chen and T.-S. Chung, *J. Phys. Chem. B*, 2005, **109**, 5638-5643; b) J. Xiong, X. Liu, J. Li, J. Narayanan and R. Wang, *Appl. Phys. Lett.*, 2006, **89**, 083106.
73. a) X. Y. Liu and P. D. Sawant, *Angew. Chem. Int. Edit.*, 2002, **41**, 3641-3645; b) J.-L. Li, X.-Y. Liu, R.-Y. Wang and J.-Y. Xiong, *J. Phys. Chem. B*, 2005, **109**, 24231-24235; c) J.-L. Li and X.-Y. Liu, *Appl. Phys. Lett.*, 2005, **87**, 113103; d) R.-Y. Wang, X.-Y. Liu, J. Narayanan, J.-Y. Xiong and J.-L. Li, *J. Phys. Chem. B*, 2006, **110**, 25797-25802; e) H.-B. Xia, X.-Y. Liu and K.-Q. Zhang, *Chem. Mater.*, 2008, **20**, 2432-2434.
74. A. P. Schenning, F. B. Benneker, H. P. Geurts, X. Y. Liu and R. J. Nolte, *J. Am. Chem. Soc.*, 1996, **118**, 8549-8552.
75. a) X. Y. Liu, P. Bennema, L. A. Meijer and M. S. Couto, *Chem. Phys. Lett.*, 1994, **220**, 53-58; b) X. Y. Liu and P. Bennema, *Phys. Rev. E*, 1993, **48**, 2006-2015; c) X. Y. Liu, *Phys. Rev. E*, 1994, **49**, 583-590; d) X. Y. Liu, *Phys. Rev. B*, 1999, **60**, 2810-2817; e) X. Y. Liu, *J. Chem. Phys.*, 1995, **102**, 1373-1384; f) X. Y. Liu, *J. Cryst. Growth*, 1997, **174**, 380-385; g) J. L. Li and X. Y. Liu, *J. Phys. Chem. B*, 2009, **113**, 15467-15472; h) X. Y. Liu, P. D. Sawant, W. B. Tan, I. B. M. Noor, C. Pramesti and B. H. Chen, *J. Am. Chem. Soc.*, 2002, **124**, 15055-15063.
76. K. Murata, M. Aoki, T. Suzuki, T. Harada, H. Kawabata, T. Komori, F. Ohseto, K. Ueda and S. Shinkai, *J. Am. Chem. Soc.*, 1994, **116**, 6664-6676.
77. K. Tsuchiya, Y. Orihara, Y. Kondo, N. Yoshino, T. Ohkubo, H. Sakai and M. Abe, *J. Am. Chem. Soc.*, 2004, **126**, 12282-12283.
78. a) Z. L. Wu, B. Ondruschka and G. Cravotto, *Environ. Sci. Technol.*, 2008, **42**, 8083-8087; b) M. M. Mojtahedi, M. Javadpour and M. S. Abaee, *Ultrason. Sonochem.*, 2008, **15**, 828-832.
79. a) C. Sanchez, H. Arribart and M. M. G. Guille, *Nat. Mater.*, 2005, **4**, 277-288; b) J. L. Atwood and J. W. Steed, *Encyclopedia of supramolecular chemistry*, CRC Press, 2004; c) N. M. Sangeetha and U. Maitra, *Chem. Soc. Rev.*, 2005, **34**, 821-836; d) T. Naota and H. Koori, *J. Am. Chem. Soc.*, 2005, **127**, 9324-9325; e) K. Isozaki, H. Takaya and T. Naota, *Angew. Chem. Int. Edit.*, 2007, **46**, 2855-2857; f) J. Wu, T. Yi, T. Shu, M. Yu, Z. Zhou, M. Xu, Y. Zhou, H. Zhang, J. Han, F. Li and C. Huang, *Angew. Chem. Int. Edit.*, 2008, **47**, 1063-1067.
80. J. M. J. Paulusse, D. J. M. van Beek and R. P. Sijbesma, *J. Am. Chem. Soc.*, 2007, **129**, 2392-2397.
81. R.-Y. Wang, X.-Y. Liu and J.-L. Li, *Cryst. Growth Des.*, 2009, **9**, 3286-3291.
82. C. Wang, D. Zhang and D. Zhu, *J. Am. Chem. Soc.*, 2005, **127**, 16372-16373.
83. J. Liu, P. He, J. Yan, X. Fang, J. Peng, K. Liu and Y. Fang, *Adv. Mater.*, 2008, **20**, 2508-2511.
84. a) O. E. Perez and A. M. Pilosof, *Food Res. Int.*, 2004, **37**, 102-110; b) N. Dubey, P. Letourneau and R. Tranquillo, *Biomaterials*, 2001, **22**, 1065-1075.
85. J.-L. Li and X.-Y. Liu, *J. Phys. Chem. B*, 2009, **113**, 15467-15472.
86. A. T. Nguyen, Q. L. Huang, Z. Yang, N. Lin, G. Xu and X. Y. Liu, *Small*, 2015, **11**, 1039-1054.
87. R. Y. Wang, X. Y. Liu and J. L. Li, *Cryst. Growth. Des.*, 2009, **9**, 3286-3291.
88. R. Y. Wang, X. Y. Liu, J. Y. Xiong and J. L. Li, *J. Phys. Chem. B*, 2006, **110**, 7275-7280.
89. a) N. Lin, X. Y. Liu, Y. Y. Diao, H. Xu, C. Chen, X. Ouyang, H. Yang and W. Ji, *Adv. Funct. Mater.*, 2012, **22**, 361-368; b) N. C. Tansil, Y. Li, C. P. Teng, S. Zhang, K. Y. Win, X. Chen, X. Y. Liu and M. Y. Han, *Adv. Mater.*, 2011, **23**, 1463-1466; c) N. Lin, Z. Meng, G. W. Toh, Y. Zhen, Y. Diao, H. Xu and X. Y. Liu, *Small*, 2015, **11**, 1205-1214.
90. a) C. Vepari and D. L. Kaplan, *Prog. Polym. Sci.*, 2007, **32**, 991-1007; b) N. Du and X. Y. Liu, in *Soft Fibrillar Materials: Fabrication and Applications*, ed. J. L. X. Y. Liu, Wiley-VCH Verlag GmbH & Co. KGaA, Weinheim, Germany, 2013, pp. 185-208; c) N. B. Lin, X. Y. Liu, H. Y. Xu, G. Y. W. Toh and J. L. Li, in *Soft Fibrillar Materials: fabrication and applications*, ed. J. L. X. Y. Liu, Wiley-VCH Verlag GmbH & Co. KGaA, Weinheim, Germany, 2013, pp. 209-231.
91. F. Vollrath, B. Madsen and Z. Shao, *Proc. R. Soc. Lond. B. Biol. Sci.*, 2001, **268**, 2339-2346.
92. N. Du, Z. Yang, X. Y. Liu, Y. Li and H. Y. Xu, *Adv. Funct. Mater.*, 2011, **21**, 772-778.
93. Z. Shao and F. Vollrath, *Nature*, 2002, **418**, 741-741.
94. G. Xu, L. Gong, Z. Yang and X. Liu, *Soft matter*, 2014, **10**, 2116-2123.
95. X. Y. Liu, *Appl. Phys. Lett.*, 2001, **79**, 39-41.
96. K. Takahashi, in *Silk polymers-Materials Science and Biotechnology*, eds. D. L. Kaplan, W. W. Adams, B. Farmer and C. viney, ACS Books, Washington, D. C., 1994.
97. N. T. M. A. Becker, in *Silk polymers-Materials Science and Biotechnology*, ed. W. W. A. D. L. Kaplan, B. Farmer, C. viney, ACS Books, Washington, D. C., 1994.
98. Y. Liu, A. Sponner, D. Porter and F. Vollrath, *Biomacromolecules*, 2008, **9**, 116-121.
99. T. Alfrey and H. Mark, *J. Phys. Chem.*, 1942, **46**, 112-118.
100. B. A. G. Schrauwen, Eindhoven University of Technology, 2003.
101. J. Moore, *Br. J. Appl. Phys.*, 1950, **1**, 6-9.
102. F. Vollrath, *Int. J. Biol. Macromol.*, 1999, **24**, 81-88.
103. C. P. Brown, C. Harnagea, H. S. Gill, A. J. Price, E. Traversa, S. Licocchia and F. Rosei, *ACS Nano*, 2012, **6**, 1961-1969.
104. H. E. Daniels, *Proceedings of the Royal Society of London. Series A. Mathematical and Physical Sciences*, 1945, **183**, 405-435.
105. Y. Termonia, *Macromolecules*, 1994, **27**, 7378-7381.
106. K. B. Broberg, *Cracks and fracture*, Academic Press, 1999.
107. T. L. Anderson, *Fracture mechanics: fundamentals and applications*, CRC press, 2005.
108. J. P. Hirth and J. Lothe, *Theory of dislocations*, Krieger Publishing Company, New York, 1982.
109. T. Lefevre, J. Leclerc, J.-F. Rioux-Dube, T. Buffeteau, M.-C. Paquin, M.-E. Rousseau, I. Cloutier, M. Auger, S. M. Gagne, S. Boudreau, C. Cloutier and M. Pezolet, *Biomacromolecules*, 2007, **8**, 2342-2344.
110. a) Z. Lin, Q. Deng, X.-Y. Liu and D. Yang, *Adv. Mater.*, 2013, **25**, 1216-1220; b) F. Teule, Y. G. Miao, B. H. Sohn, Y. S. Kim, J. J. Hull, M. J. Fraser, R. V. Lewis and D. L. Jarvis, *Proc. Natl. Acad. Sci. U. S. A.*, 2012, **109**, 923-928.